NACA TN 4261

NATIONAL ADVISORY COMMITTEE FOR AERONAUTICS

TECHNICAL NOTE 4261

ACOUSTIC, THRUST, AND DRAG CHARACTERISTICS OF SEVERAL FULL-SCALE NOISE SUPPRESSORS FOR TURBOJET ENGINES

By Carl C. Ciepluch, Warren J. North, Willard D. Coles and Robert J. Antl

Lewis Flight Propulsion Laboratory
Cleveland, Ohio

Washington
April 1958

NATIONAL ADVISORY COMMITTEE FOR AERONAUTICS

TECHNICAL NOTE 4261

ACOUSTIC, THRUST, AND DRAG CHARACTERISTICS OF SEVERAL FULL-SCALE NOISE SUPPRESSORS FOR TURBOJET ENGINES

By Carl C. Ciepluch, Warren J. North, Willard D. Coles and Robert J. Antl

SUMMARY

An experimental investigation was conducted to determine the acoustic, internal thrust, and external drag characteristics of several full-scale turbojet-exhaust noise suppressors on an engine in the 10,000-pound-thrust class. Acoustic measurements were made around an outdoor thrust stand. The thrust and drag data were obtained in an altitude wind tunnel over a range of Mach numbers up to 0.5.

The most efficient configurations were a two-position mixing nozzle with ejector and a 12-lobe nozzle, considering both exhaust-jet noise reduction and loss in engine propulsive thrust due to either internal thrust losses or afterbody-drag increases. At a Mach number of 0.5 the respective propulsive thrust losses were about 1 and 3 percent. Calculations indicate that, from the standpoint of the ground observer, the aircraft takeoff noise from these two suppressors should be 5 or 6 decibels less than that of the standard convergent nozzle.

INTRODUCTION

The noise levels of turbojet-powered transport aircraft are considerably greater than those of current piston-engine-powered transports. Considerable analytical and experimental research has been done to find means of reducing the noise levels of the turbojet transports. Noise levels can be decreased by engine redesign to reduce the jet-exit velocity (ref. 1), proper flight-climb techniques (ref. 2), and the use of noise-suppression exhaust nozzles (refs. 3 to 5). The present report is concerned with the last method.

The selection of a suitable turbojet-exhaust sound suppressor depends on considerations of (1) sound-suppression ability, (2) internal thrust, and (3) external drag characteristics. A significant decrease in propulsive thrust would cause a critical reduction in aircraft range

or payload. The propulsive thrust characteristics of an engine installation with a suppressor are a function of both internal and external nozzle characteristics. The internal performance is a function of the losses caused by flow separation and friction, which reduce the total pressure of the jet exhaust and thereby reduce the thrust. The external suppressor drag is composed of afterbody or boattail drag and wing-suppressor interference drag. The afterbody drag is related to the pressure distribution on the aft surfaces of the suppressor nozzle and the friction drag that arises from viscous flow over the nozzle.

Little information is available on the aerodynamic performance of full-scale noise suppressors. Consequently, an investigation was conducted at the Lewis laboratory to determine the acoustic, internal thrust, and external drag characteristics of several full-scale exhaust-jet noise suppressors that are representative of proposed flight configurations. The investigation was conducted in two parts on nonafterburning turbojet engines of the 10,000-pound-thrust class. Acoustic data were obtained around an outdoor test stand. Thrust and drag measurements were obtained over a range of flight speeds and altitudes in the Lewis altitude wind tunnel. Limited acoustic measurements were also obtained during the altitude wind tunnel investigation.

The acoustic characteristics of the suppressors and a standard convergent-nozzle configuration are compared in terms of polar sound-pressure level, spectrum level, power-spectrum level, total-sound-power level, and an intensity- and duration-annoyance parameter. The aerodynamic characteristics of the suppressors and the standard configuration are compared in terms of internal performance (thrust coefficient) and external drag (total-drag coefficient and boattail-drag coefficient).

APPARATUS AND PROCEDURE

The engines used during the free-field (test-stand) and wind-tunnel tests were identical models that produced approximately 9000 pounds of sea-level static thrust at a nozzle pressure ratio of 2.2.

Free-Field Facility

Installation. - The engine was installed on an outdoor test stand (fig. 1(a)) with the engine centerline 8 feet above the ground plane. The test stand, control room, and noise-field survey stations were oriented as shown in figure 1(b). With the exception of the ground and the control room, the nearest sound-reflection surface was a building 600 feet directly in front of the engine.

Instrumentation. - The engine was mounted by flexure plates to permit strain-gage thrust measurements. Engine airflow, fuel flow, rotor speed, and exhaust pressures and temperatures were measured and recorded. Wind direction and velocity were measured at the test site.

Sound-pressure levels were measured with a commercial sound-level meter that had a flat frequency response from 20 to 10,000 cycles per second. Jet noise-spectrum data were obtained with an automatic audio-frequency analyzer and recorder. The frequency range of this instrument was 40 to 16,000 cycles per second and was divided into 27 one-third-octave bands. The spectrum analyzer and recorder were mounted in an acoustically insulated truck in order that direct field records could be obtained. Before each test, both the sound-level meter and the frequency analyzer were calibrated with a small loudspeaker-type calibrator and transistor oscillator.

Procedure. - Acoustic measurements were made 8 feet above ground level at a radial distance of 200 feet from the engine exhaust in increments of 15° over a 270° sector. As shown in figure 1(b), no acoustic measurements were made in the forward quadrant where the control room was located, and no tests were made when the wind velocity was greater than 12 miles per hour. No spectrum data above 10,000 cycles per second are presented herein because the spectrum content of turbojet noise is insignificant at these frequencies.

The sound data were taken at 86 percent of sea-level rated thrust with the standard nozzle in order that comparisons at constant thrust could be made over a range of ambient temperatures. In order to determine whether the acoustic data would need to be corrected, the effect of atmospheric temperature and pressure variations on exhaust-jet noise was calculated. The sound power of a simple convergent nozzle is proportional to the parameter $\rho_0 A V^8 / a_0^5$ (ref. 6); this relation was assumed to be correct also for any given suppressor nozzle (all symbols are defined in appendix A). By using generalized engine-performance parameters and this acoustic parameter, it was determined that for constant thrust the greatest variations encountered in atmospheric conditions would change the measured acoustic properties by less than 0.3 decibel. Therefore, no atmospheric corrections were made to the acoustic data presented.

Sound-pressure level is defined herein as the root-mean-square value of the sound pressure. The sound-pressure level is given in decibels and is referenced to a pressure of 2×10^{-4} dyne per square centimeter. Spectrum level at a specified frequency is the sound pressure within a band 1-cycle-per-second wide centered at the frequency. The total-sound-power level is obtained from a hemispherical integration of sound-pressure level about the engine and represents all the sound power radiated from the engine. Total-sound-power level is given in decibels and is

referenced to a power of 10^{-13} watt. Power-spectrum level at a specified frequency is the portion of total-sound-power level in a band 1-cycle-per-second wide centered at the frequency.

Altitude Wind Tunnel

Installation. - A photograph of the engine installation in the wind tunnel is shown in figure 2(a). The closed-circuit tunnel has a 20-foot-diameter test section. The tunnel fan produced Mach numbers in the tunnel test section up to 0.33 at a simulated altitude of 15,000 feet, and 0.5 at 40,000 feet. Tunnel refrigeration was available to simulate the low temperatures required for altitude operation. The engine was mounted on a vertical strut directly connected to the tunnel scale system in order to obtain scale thrust measurements. An aircraft nacelle fairing approximately 14 feet long enclosed the engine. Engine exhaust was removed from the tunnel air with an exhaust scoop downstream of the engine. The engine nacelle and strut blocked 6.5 percent of the test-section cross-sectional area.

Instrumentation. - The amount and the location of the instrumentation used to determine the drag and internal thrust losses are shown in figure 2(b). The free-stream total and static pressure and the engine fuel flow and speed were also measured. A total of 40 static-pressure taps, which surveyed both axial and circumferential pressure distributions, were provided on the standard nozzle boattail. The standard configuration is shown in figure 3. Tunnel acoustic measurements were made with five strut-mounted microphones located at four axial positions with respect to the engine.

Procedure. - Nozzle internal performance was determined during sea-level static runs for which the engine cowl inlet was replaced with a bellmouth-type inlet. Scale thrust readings and engine parameters were obtained over a range of nozzle pressure ratios, and the nozzle thrust coefficients were calculated as described in appendix B.

Nacelle and boattail-drag measurements were obtained for simulated free-stream Mach numbers of 0.15, 0.23, and 0.33 at an altitude of 15,000 feet, and for 0.4 and 0.5 at an altitude of 40,000 feet. Drag data were obtained for a range of engine speeds at these simulated flight conditions, and the drag coefficients were calculated as described in appendix B.

Noise Suppressor Configurations

The following nozzle configurations were investigated:

Configuration	Description	Cross section in figure -
Standard	Convergent nozzle	3
A	12-Lobe	4(a)
B	12-Lobe with centerbody	4(b)
C	Segmented lobe	4(c)
D	10-Tube, rectangular exits	4(d)
E	11-Tube, circular exits	4(e)
F	31-Tube, circular exits	4(f)
G[a]	Standard with ejector	4(g)
H	Mixing nozzle with ejector	4(h)

[a]Configuration G is considered the cruise position of a variable-geometry suppressor (configuration H).

The engine had a fixed tailcone section downstream of the turbine that was approximately 15 inches long and included the aft bearing support. Therefore, it was necessary to design all the nozzles to conform to the outlet diameter of this section; this resulted in some divergence of the flow passage aft of the attachment flange. Turbine-outlet instrumentation was located in the fixed section of the tailcone, and each nozzle was attached to the fixed tailcone section.

Because the nozzles had different shapes, the nacelle had to be modified to accept each nozzle. To do this, the original nacelle was arbitrarily cut off at a point approximately $5\frac{1}{2}$ inches downstream of the turbine, and additional sections of fairings were fabricated to fit between the original nacelle fairing and the nozzles. The modified section of the nacelle for each nozzle is included in the cross-sectional views in figure 4.

RESULTS AND DISCUSSION

Evaluation of exhaust-jet noise suppressors must include considerations of noise-suppression effectiveness, reductions in engine thrust, and increases in suppressor-afterbody drag. Engine thrust reductions and afterbody-drag increases are important factors because they indirectly affect either aircraft range or payload. In evaluating the noise suppressors reported herein, the acoustic qualities are examined first, followed by a comparison of the thrust and drag performance. Finally, selection of the most promising noise suppressors is made on the basis of both the noise-suppression effectiveness and the thrust and drag performance. In

order to simplify the presentation of the data, the noise-suppression nozzles are divided into three general groups: lobe (configurations A, B, and C), tube (D, E, and F), and ejector-type (G and H) nozzles.

Acoustic Characteristics

Acoustic data are presented in terms of the sound-pressure levels, spectrum levels, and power-spectrum levels in figures 5 to 11 and are briefly discussed in the following section. Summary plots involving some of these acoustic data are presented in figures 12 to 14 and are discussed in the Analysis of Free-Field Data.

Free-field test data. -

Lobe-type nozzles (configurations A, B, and C): The sound characteristics of the three lobe-type nozzles are shown in figures 5 to 7. The 12-lobe nozzle (fig. 5(a)) produced sound-pressure levels at all stations around the engine that were lower than those of the standard nozzle, while the other two configurations (figs. 5(b) and (c)) indicated increased levels in some sectors. The peak reduction (7 db) in sound-pressure level occurred with the centerbody nozzle at an azimuth of 30°. Little suppression was obtained with the segmented lobe (fig. 5(c)).

In general, the decrease in peak spectrum levels (fig. 6) at the three azimuths corresponds to the decrease at the respective azimuths of the sound pressures presented in the polar sound patterns. The most marked change in the spectrum levels occurred at the 30° axis for frequencies from 100 to 1000 cycles per second. All three nozzles showed a reduction at the 30° azimuth, with a maximum spectrum-level attenuation of 29 decibels at 315 cycles per second for the centerbody-lobe configuration (fig. 6(b)). Above about 1000 cycles per second, all lobe configurations produced higher spectrum levels at all azimuths.

Figure 7 shows the power-spectrum level as a function of frequency. The 12-lobe nozzles (configurations A and B) produced significant reductions in the frequency range below 1000 cycles per second. Although the suppressor power-spectrum level was greater above 1000 cycles per second, the levels were sufficiently low to contribute little to total sound power. The spectrum content of sound power of the segmented lobe (fig. 7(c)) was similar to that of the standard nozzle.

Tube nozzles (configurations D, E, and F): Although the tubular configurations reduced the sound-pressure levels behind the engine (9 db for the 10-tube nozzle), they caused increases in the sound-pressure levels at angles greater than 65° to the jet axis (fig. 8). In fact, the 10-tube nozzle (fig. 8(a)) produced sound-pressure levels at 75° that were as high as those at 45°.

The spectrum level for the 10-tube nozzle (fig. 9(a)) showed reductions at the 30° azimuth for noise frequencies below 1000 cycles per second. At 30° the 11- and 31-tube nozzles (figs. 9(b) and (c)) caused spectrum-level reductions for frequencies from 100 to 1000 cycles per second. However, at frequencies above 1000 cycles per second and for all frequencies at azimuths of 90° and 150°, the tubular nozzles produced higher spectrum levels than the standard nozzle.

Figure 10(a) indicates that the power-spectrum level was reduced 8 to 10 decibels in the critical frequency range (100 to 300 cps) for the 10-tube nozzle. However, the power-spectrum level was so increased at higher frequencies that nearly uniform spectrum power existed in a range from 40 to 1250 cycles per second. The 11- and 31-tube configurations (figs. 10(b) and (c)) showed similar power-spectrum trends, but the low-frequency sound attenuation was less than with the 10-tube nozzle.

Ejector (configuration H): Sound measurements of the mixing nozzle and ejector (configuration H) are presented in figure 11. No static sound measurements were taken with the standard nozzle and ejector (configuration G), because reference 7 shows that little sound reduction is to be gained with this configuration.

The sound pressures at the 35° azimuth were reduced 7 decibels by the mixing nozzle-ejector combination (fig. 11(a)). Essentially no decrease in sound pressure occurred at angles greater than 70°.

The spectrum levels at 30° were below those for the standard nozzle at all frequencies less than 2500 cycles per second (fig. 11(b)). The spectrum levels for the suppressor nozzle were slightly higher than those of the standard configuration at the 90° and 150° azimuths.

For frequencies below 500 cycles per second, the power-spectrum level (fig. 11(c)) reflects the spectrum-level trends at the 30° azimuth; this indicates that much of the low-frequency noise has been reduced. The suppressor nozzle increased the power-spectrum level at frequencies above 500 cycles per second.

Analysis of free-field data. - A complete acoustic evaluation of the various suppressors would involve determination of frequency distribution of noise, polar sound pressures, noise duration during flight operations, total-sound-power level, atmospheric attenuation, and various physiological and psychological considerations. However, a few comparisons that will immediately group those configurations of most interest can be made.

Total sound power: A total-sound-power comparison is made in figure 12. Four nozzles - 10-tube, 12-lobe with centerbody, 12-lobe, and mixing nozzle with ejector - produced total-sound-power levels that were

2.7 to 4.3 decibels less than that of the standard nozzle. The remaining configurations produced total-sound-power levels nearly the same as that of the standard nozzle.

Sound levels from aircraft in flight: The polar sound fields presented are the sound levels an observer would hear while walking around a turbojet engine at a radius of 200 feet. However, during a takeoff pass, the stationary observer will hear different polar-sound variations. Calculations were made to determine the sound pressures transmitted to a ground observer from a 40,000-pound-thrust airplane at an altitude of 500 feet and an airspeed of 200 knots. The polar sound pressures from figures 5 to 11 were corrected for thrust, aircraft flight speed (ref. 2, equal correction assumed for all nozzles), and inverse-square-distance attenuation.

The resulting sound-pressure levels were converted to loudness (sones) and are shown in figure 13. Numerous complexities are involved in determining a realistic value for jet-noise loudness. Since most of the jet noise occurs at frequencies between 100 and 1600 cycles per second, the conversion to sones was approximated by use of the mean value of the curves for 100 to 1600 cycles per second in figure 18 of reference 8. Using figures 13(a) and (b), one can determine not only the peak loudness caused by the various nozzles but also the differences due to noise duration. All the suppressors reduced the peak loudness below that of the standard nozzle. The greatest reduction, about 40 sones (equivalent to 5 or 6 decibels), was obtained with the 12-lobe nozzle (A) and the mixing nozzle with ejector (H).

Integrating the area under the respective curves yields numbers that can be used for a first-order estimation of loudness and duration annoyance. The loudness-and-duration annoyance values were determined by integrating the loudness area above 50 sones. A comparison of the nozzles based on this integration is shown in figure 14. Again, the same grouping is possible as for total sound power (fig. 12). The 10-tube and the ejector configuration appear to be the best nozzles from an annoyance consideration. The merit of the 10-tube nozzle is the rapid reduction in observed loudness after the aircraft passes overhead.

Among the suppressors tested, the better acoustic configurations appear to be the two 12-lobe types, the 10-tube, and the mixing nozzle with ejector; however, the final evaluation will also depend on thrust and drag characteristics.

Altitude-wind-tunnel sound measurements. - The wind-tunnel acoustic measurements were of limited value because of tunnel background noise and an exhauster intake scoop that distorted the jet-exhaust spreading pattern. However, trends in the acoustic data indicate that at constant jet thrust or jet velocity there is a reduction in sound pressure as flight speeds increase. The tunnel data also indicate that the lobe-type

nozzles show somewhat greater reduction in sound pressures with increasing flight speeds than do the other nozzles.

Aerodynamic Performance

Internal performance. - The internal performance of the various noise-suppression nozzles is compared with that of the standard nozzle in figure 15. The internal performance is presented as a thrust coefficient, which is defined as the ratio of the actual jet velocity to ideal jet velocity. The nozzle pressure ratio, from which the ideal jet velocity is obtained, is the ratio of turbine-outlet total pressure to nozzle ambient static pressure. The thrust coefficient therefore includes the losses in potential jet velocity due to tailpipe pressure losses as well as the internal aerodynamic losses attributable to the exhaust nozzle itself.

The peak thrust coefficient of the standard nozzle was 0.975. At a nozzle pressure ratio of 2.2, the thrust coefficients of the lobe-type nozzles were from 3 to 5.5 points lower than that of the standard nozzle. This decrease in thrust coefficient resulted from increased tailpipe pressure losses and increased nozzle friction losses due to the increased wetted area.

The tube-type noise-suppression nozzles exhibited severe losses in thrust coefficient (fig. 15(b)). At a nozzle pressure ratio of 2.2, the thrust coefficients of the 10-, 11-, and 31-tube nozzles were 0.880, 0.895, and 0.865, respectively, which represents an 8- to 11-point reduction in thrust coefficient below that of the standard nozzle. A large part of this loss in thrust coefficient is a result of flow separation in the tailpipe just ahead of the nozzle tubes. This flow separation is not inherent in tubular nozzles, but was due to undesirable variations of the tailpipe flow area as mentioned in APPARATUS AND PROCEDURE. Total-pressure instrumentation at the nozzle discharge indicated that the flow separation resulted in severe total-pressure losses in the outer ring of tubes for the 11- and 31-tube nozzles and in the corner tubes for the 10-tube nozzle. The high tailpipe total-pressure losses for the tube nozzles resulted in a pronounced increase in nozzle thrust coefficient with increasing nozzle pressure ratio.

The thrust coefficient of the mixing nozzle both with and without the ejector shroud is shown in figure 15(c). The mixing nozzle alone had relatively large losses in thrust coefficient compared with the

standard nozzle; this probably resulted from over-expansion or an aspirating effect of the exhaust jet on the diverging mixing flaps. The thrust coefficient of the mixing nozzle was 5 points lower than that of the standard nozzle at a nozzle pressure ratio of 2.2. The ejector shroud augmented the thrust of the mixing nozzle with the result that the thrust coefficient was approximately equal to that of the standard nozzle.

The internal losses of the ejector nozzles during simulated flight conditions could not be evaluated directly because of the differences in secondary flow conditions during static calibration and tunnel tests. The thrust loss or gain attributable to the ejector shroud for simulated flight conditions is contained in the drag coefficient of the ejector nozzle, since the engine thrust based on the primary nozzle thrust coefficient was used in conjunction with measured thrust minus drag to determine the boattail drag (see appendix B). Although the static tests of the ejector configuration indicated that the ejector shroud augmented the primary nozzle thrust during flight there may be losses in nozzle propulsive thrust due to the presence of the ejector shroud.

With the exception of the mixing nozzle with ejector, the thrust coefficients of the noise-suppression nozzles ranged from 3 to 11 points lower than that of the standard nozzle at a nozzle pressure ratio of 2.2. This loss was due to the increased wetted area or the friction losses and total-pressure losses in the tailpipe and nozzle entrance. Increased wetted area is a characteristic of most noise-suppression nozzles; therefore, some resulting friction losses are unavoidable. However, tailpipe pressure losses and entrance losses can be kept to a minimum by following good aerodynamic design of the tailpipe and nozzle combination.

External drag characteristics. - In order to obtain the suppressor boattail drag, it was necessary to first determine the total nacelle drag. The effect of inlet mass-flow ratio on total nacelle drag was then investigated. Even though the Mach number range investigated was relatively small, the nacelle inlet operated over a wide range of mass-flow ratios (ratio of engine airflow to airflow of free-stream tube equal to inlet cross-sectional area). A typical set of data for the standard nozzle, showing the effect of free-stream Mach number and engine speed on the total nacelle drag and inlet mass-flow ratio, is shown in figure 16. At a Mach number of 0.33, for example, the drag coefficient increased from 0.085 to 0.135 as the engine speed was increased from 90 to 104 percent. Similarly, the mass-flow ratio increased from 0.7 to 0.88. Most of the change in drag coefficient resulted from changes in

inlet-lip pressure distribution caused by the change in mass-flow ratio, as illustrated in the following sketch:

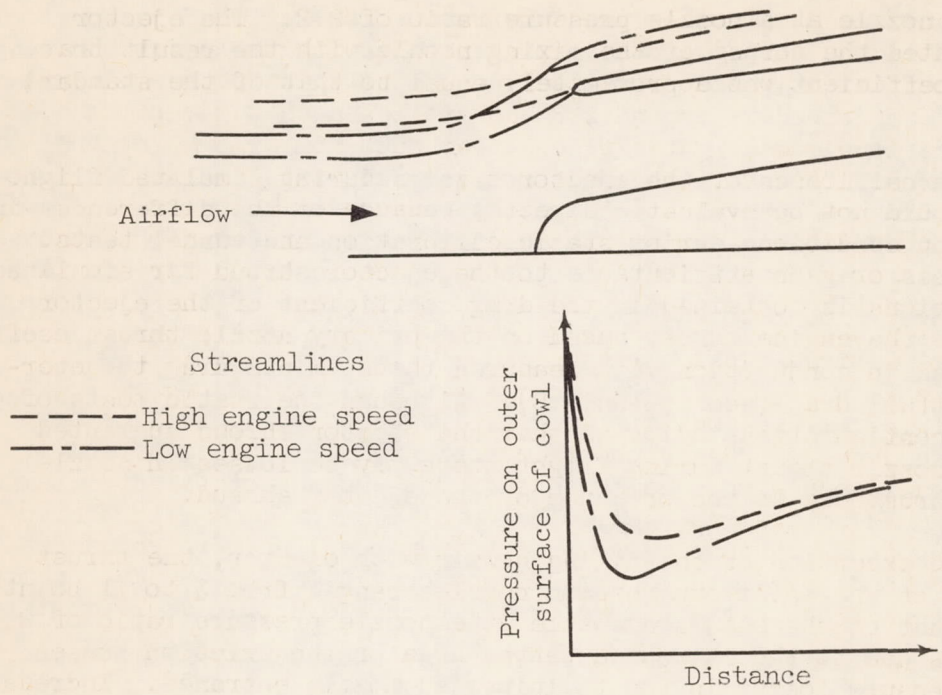

At low engine speeds (low mass-flow ratios), the velocity over the lip of the nacelle was high, which resulted in a low static pressure or low drag; at high engine speeds (high mass-flow ratio), the velocity over the lip was lower, which resulted in an increased static pressure and drag. The total drag data presented in this report are for a constant corrected engine speed of 104.5 percent of rated. As the free-stream Mach number increased, the inlet mass-flow ratio decreased sharply; this resulted in a decrease in drag coefficient. However, the mass-flow ratio is the same for all configurations at a given engine speed and free-stream Mach number and, therefore, does not affect comparisons of the total drag coefficients of the configurations.

The total drag coefficients obtained with the noise-suppression nozzles and the standard nozzle are shown for a constant corrected engine speed in figure 17. In general, the drag coefficients of the lobe-type configurations were approximately equal to that of the standard nozzle, whereas the tube-type and ejector-type configurations caused substantial increases in drag coefficient. At a Mach number of 0.5 the drag coefficient of the standard nozzle and the lobe-type configurations was 0.07, while drag coefficients from 0.10 to 0.15 were obtained for the tube-type nozzles, and 0.125 for the ejector-type nozzles.

Any differences in total drag coefficient from that of the standard nozzle are directly attributable to a change in afterbody or boattail drag, since the drag of the nacelle ahead of the boattail should remain constant at a given Mach number and inlet mass-flow ratio. A comparison of the boattail-drag coefficients is presented in figure 18 for the range of Mach numbers investigated. Boattail-drag coefficients were determined by the method described in appendix B and are based on the maximum boattail cross-sectional area. At a free-stream Mach number of 0.5, the boattail-drag coefficient of the standard and lobe-type nozzles was 0.04, the boattail drag of the tube-type nozzles ranged from 0.07 to 0.14, and the boattail-drag coefficient of the ejector nozzles was 0.11. The observed boattail-drag coefficients of the tube- and ejector-type nozzles were, therefore, from 2 to $4\frac{1}{2}$ times greater than that of either the standard nozzle or the lobe-type nozzles.

Figure 19 gives the boattail drag as a percent of the engine net thrust for the range of Mach numbers investigated. In order to compare the drag of each nozzle on a common basis, the engine net thrust obtained with the standard nozzle was used. The comparison is made with the engine operating at a constant corrected engine speed, near rated, and, therefore, would approximate a climb-flight condition for the Mach number range presented. The boattail drag of the standard nozzle and lobe-type nozzles was approximately $1\frac{1}{2}$ percent of the net thrust at a Mach number of 0.5. The boattail drag of the tube nozzles was about 3.0 to 6.5 percent of the net thrust. The ejector nozzles caused a boattail drag which was approximately 5.0 percent of the net thrust. Although there appears to be a substantial penalty in net thrust due to the increase in boattail drag of the tube and ejector nozzles at a Mach number of 0.5, extrapolation of the data indicates that even more severe penalties due to drag may be incurred at aircraft cruise Mach numbers of 0.8 to 0.9.

Combined thrust and drag characteristics. - A propulsive thrust comparison was made directly from the tunnel-balance-scale readings. The tunnel scales, which indicate propulsive thrust (net thrust minus drag), provide a direct means of evaluating the suppressors at nozzle pressure ratios greater than those attainable during the static nozzle calibrations. Figure 20 shows the percent decrease, with respect to the standard convergent nozzle, in propulsive thrust for the various suppressors at a nozzle pressure ratio of 2.6. This comparison was made at 0.5 Mach number and 40,000-feet altitude, which were the highest Mach number and altitude of the test series. The actual balance-scale readings had to be adjusted in order to compensate for small variations in test-section inlet conditions and for variations in engine thrust due to differences in exhaust-nozzle effective area.

As shown in figure 20, all noise-suppression nozzles produced a reduction in propulsive thrust. Of the four most promising nozzles from

a noise-suppression standpoint (12-lobe, 12-lobe centerbody, 10-tube, and mixing nozzle with ejector), the 12-lobe nozzle produced the smallest penalty in propulsive thrust (3.2 percent at a 0.5 Mach number). The 12-lobe centerbody and 10-tube nozzles produced 6.5 and 8.6 percent reductions in propulsive thrust, respectively. It should be pointed out that the propulsive thrust loss for the lobe and tube-type nozzles was due primarily to increased internal thrust losses and that the internal thrust loss for these nozzles probably can be reduced.

The mixing nozzle with ejector, which also had good noise-suppression qualities, produced a large loss in propulsive thrust (fig. 20) resulting primarily from the large internal thrust losses of the mixing nozzle itself (fig. 15). Improvement in the ejector nozzle can be made, however, by making the mixing flaps movable and by simulating the simple standard nozzle during flight cruise conditions. This variable-geometry configuration would reduce the penalty in propulsive thrust to less than 1 percent (fig. 20) at a Mach number of 0.5 and nozzle pressure ratio of 2.6. The ejector shroud also could be retracted into the nacelle to further reduce the propulsive thrust loss during cruise conditions. However, the ejector-type noise suppressor is inherently heavier than the lobe-type nozzles (particularly if retractable flaps and shroud are used), and final evaluation then would depend on the aircraft performance penalty due to increased weight.

SUMMARY OF RESULTS

The following results were obtained during an investigation of the acoustic, drag, and thrust properties of several exhaust-jet noise suppressors:

1. With respect to sound directionality, spectrum, duration, and total sound power the better suppressors of the group tested were the 12-lobe, 12-lobe with centerbody, 10-tube, and the mixing nozzle with ejector. During aircraft takeoff, a ground observer should hear the lowest peak noise levels from the 12-lobe and the ejector mixing nozzles. The observed levels would be 5 to 6 decibels less than those obtained with the standard nozzle. The mixing nozzle with ejector produced the lowest total sound power, which was 4.3 decibels less than that of the standard nozzle.

2. Of the fixed-geometry nozzles, the 12-lobe nozzle caused the smallest penalty in propulsive thrust. This reduction amounted to 3.2 percent at a flight Mach number of 0.5. The two ejector configurations that simulated the two positions of a variable-geometry nozzle had good acoustic qualities and low propulsive thrust losses but may be handicapped because of an increased weight penalty.

3. Up to a flight Mach number of 0.5, most of the decrease in propulsive thrust resulted primarily from internal thrust losses. For the lobe-type nozzles, no increase in drag was noted. A large part of the internal thrust losses was a result of tailpipe pressure losses ahead of the nozzle.

Lewis Flight Propulsion Laboratory
National Advisory Committee for Aeronautics
Cleveland, Ohio, January 13, 1958

APPENDIX A

SYMBOLS

A	area, sq ft
A_{max}	maximum cross-sectional area of nacelle, 13.2 sq ft
$A_{max,B}$	maximum cross sectional area of boattail, 9.4 sq ft
a_o	speed of sound in ambient air, ft/sec
C_D	total drag coefficient
$C_{D,B}$	boattail drag coefficient
C_t	thrust coefficient
D	drag, lb
F_n	net thrust, lb
F_s	thrust scale reading, lb
g	acceleration due to gravity, ft/sec^2
M_O	free-stream Mach number
p_O	free-stream static pressure, lb/sq ft abs
q_O	$1/2\ p_O \gamma M_O^2$
T	total temperature, ^oR
V	velocity, ft/sec
w_a	airflow, lb/sec
w_f	fuel flow, lb/sec
γ	ratio of specific heats
ρ_O	ambient-air density, slug/cu ft

Subscripts:

i	ideal
j	jet
O	free-stream

APPENDIX B

CALCULATIONS

Airflow

The engine airflow was calculated from temperature and pressure measurements obtained at the airflow measuring station just ahead of the compressor with the following relation:

$$w_a = \frac{pAV}{RT}$$

The velocity at the measuring station was determined by the one-dimensional-flow relation described in reference 9.

Thrust

The nozzle thrust coefficient is defined as

$$C_t = \frac{\text{actual jet thrust}}{\text{ideal jet thrust}}$$

For a sea-level static run with a bellmouth on the engine inlet, the actual jet thrust is equal to the scale thrust reading F_s or

$$C_t = \frac{F_s}{\frac{w_a + w_f}{g} V_{j,i}}$$

The ideal jet velocity $V_{j,i}$ was based on the ratio of turbine-outlet total pressure to nozzle ambient static pressure, and turbine-outlet temperature. Since the airflow used in the ideal-jet-thrust term was the measured value, the thrust coefficient is actually a ratio of the effective jet velocity to an ideal jet velocity based on turbine-outlet conditions.

Drag

Drag can be expressed

$$D = F_n - F_s$$

where

$$F_n = \frac{w_a + w_f}{g} V_{j,i} C_t - \frac{w_a}{g} V_0$$

Therefore,

$$D = \left(\frac{w_a + w_f}{g} V_{j,i} C_t - \frac{w_a}{g} V_0 \right) - F_s$$

The total drag coefficient is defined as

$$C_D = \frac{D}{A_{max} q_0}$$

Evaluation of the drag of the ejector nozzles was complicated by the fact that the thrust coefficient of the ejector nozzle could not be obtained for the ejector secondary pressure ratios above 1.0 during a static calibration of the nozzle thrust coefficient. As a result, the engine net thrust with the ejector nozzles was based on the primary nozzle thrust coefficient and pressure ratio. Therefore, the drag coefficient of the ejector nozzles includes the loss or increased thrust attributable to the ejector shroud.

The boattail of each nozzle was considered as all the external surface downstream of the fixed part of the nacelle, as shown in the following sketch:

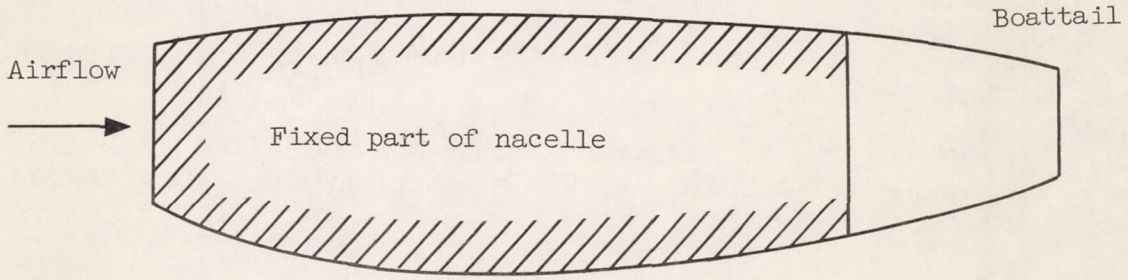

The boattail was different for each nozzle because of the different shapes of the nozzles. A cross section of the boattail shape of each nozzle is shown in figures 3 and 4.

Boattail drag coefficients were determined by subtracting the drag of the fixed part of the nacelle from the total drag

$$C_{D,B} = \frac{D_{(total)} - D_{(fixed\ part\ of\ nacelle)}}{A_{max,B} q_0}$$

An estimate of the drag of the fixed part of the nacelle was made by determining the drag of the standard-nozzle boattail and subtracting it from the total drag:

$$D_{(\text{fixed part of nacelle})} = D_{\text{total(standard nozzle)}} - D_{\text{boattail(standard nozzle)}}$$

The drag of the fixed part of the nacelle is a function of the free-stream Mach number and engine mass-flow ratio; therefore, the drag was evaluated at the same Mach number and mass-flow-ratio conditions at which total drag was obtained. The boattail drag of the standard nozzle is

$$D_{\text{boattail}} = \text{pressure drag} + \text{friction drag}$$

The pressure-drag term was evaluated from boattail static-pressure integrations. The friction-drag term was estimated from data of reference 10.

The free-stream Mach number was determined from static- and total-pressure measurements upstream of the engine. The effect of tunnel blockage on tunnel effective Mach number was not considered.

REFERENCES

1. Silverstein, Abe, and Sanders, Newell D.: Concepts on Turbojet Engines for Transport Application. Preprint No. 727, SAE, 1956.

2. North, Warren J.: Effect of Climb Technique on Jet-Transport Noise. NACA TN 3582, 1956.

3. Coles, Willard D., and Callaghan, Edmund E.: Full-Scale Investigation of Several Jet-Engine Noise-Reduction Nozzles. NACA TN 3974, 1957.

4. Greatrex, F. B.: Jet Noise. Preprint No. 559, Inst. Aero. Sci., June 1955.

5. Withington, Holden W.: Silencing the Jet Aircraft. Aero. Eng. Rev., vol. 15, no. 4, Apr. 1956, pp. 56-63; 84.

6. Coles, Willard D., and Callaghan, Edmund E.: Investigation of Far Noise Field of Jets. II - Comparison of Air Jets and Jet Engines. NACA TN 3591, 1956.

7. North, Warren J., and Coles, Willard D.: Effect of Exhaust-Nozzle Ejectors on Turbojet Noise Generation. NACA TN 3573, 1955.

8. Stevens, S. S.: Calculation of the Loudness of a Complex Noise. Jour. Acous. Soc. Am., vol. 38, no. 5, Sept. 1956.

9. Turner, L. Richard, Addie, Albert N., and Zimmerman, Richard H.: Charts for the Analysis of One-Dimensional Steady Compressible Flow. NACA TN 1419, 1948.

10. Blasius, H.: The Boundary Layers in Fluids with Little Friction. NACA TM 1256, 1950.

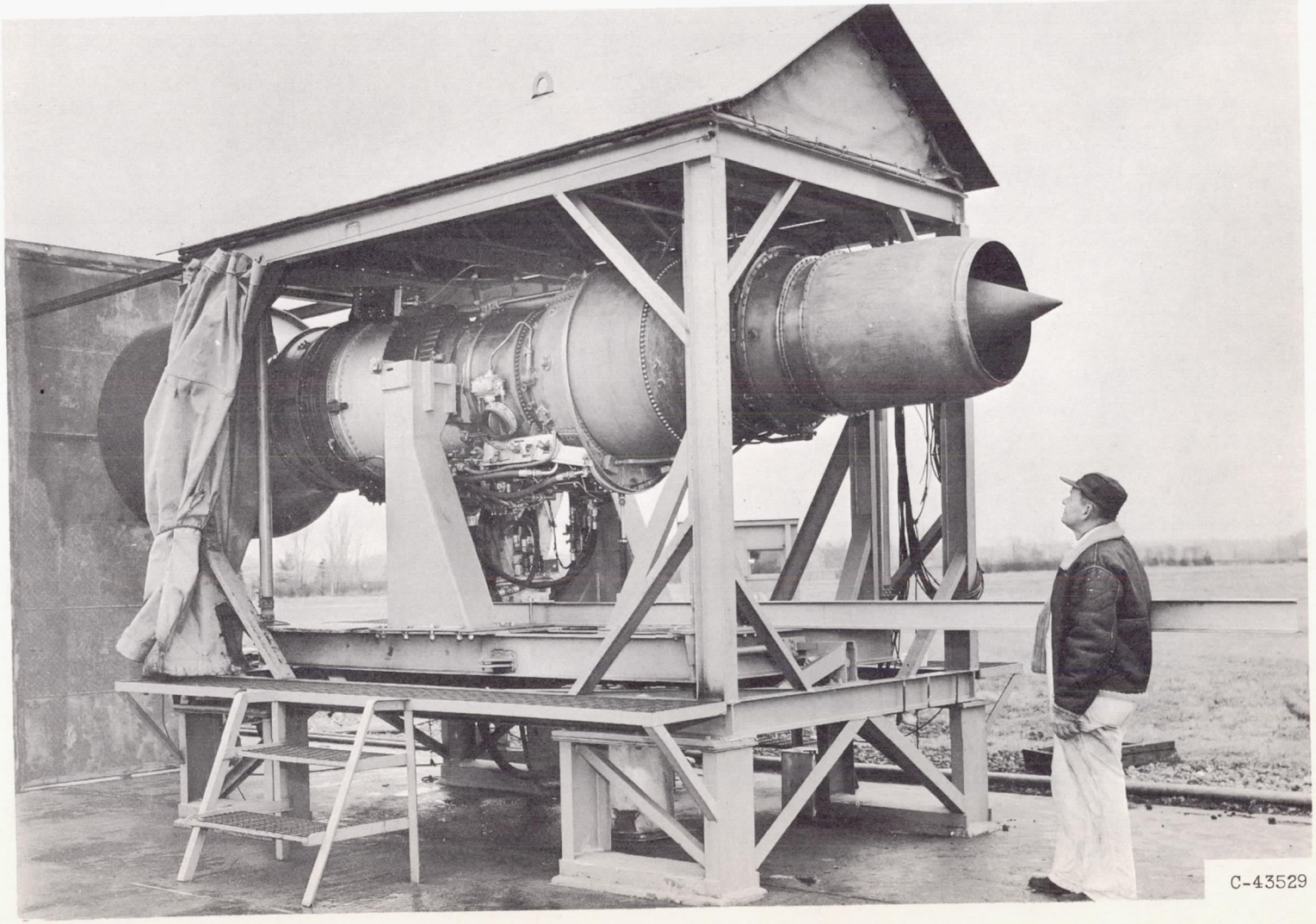

(a) Engine installed on test stand.

Figure 1. - Free-field arrangement for noise surveys.

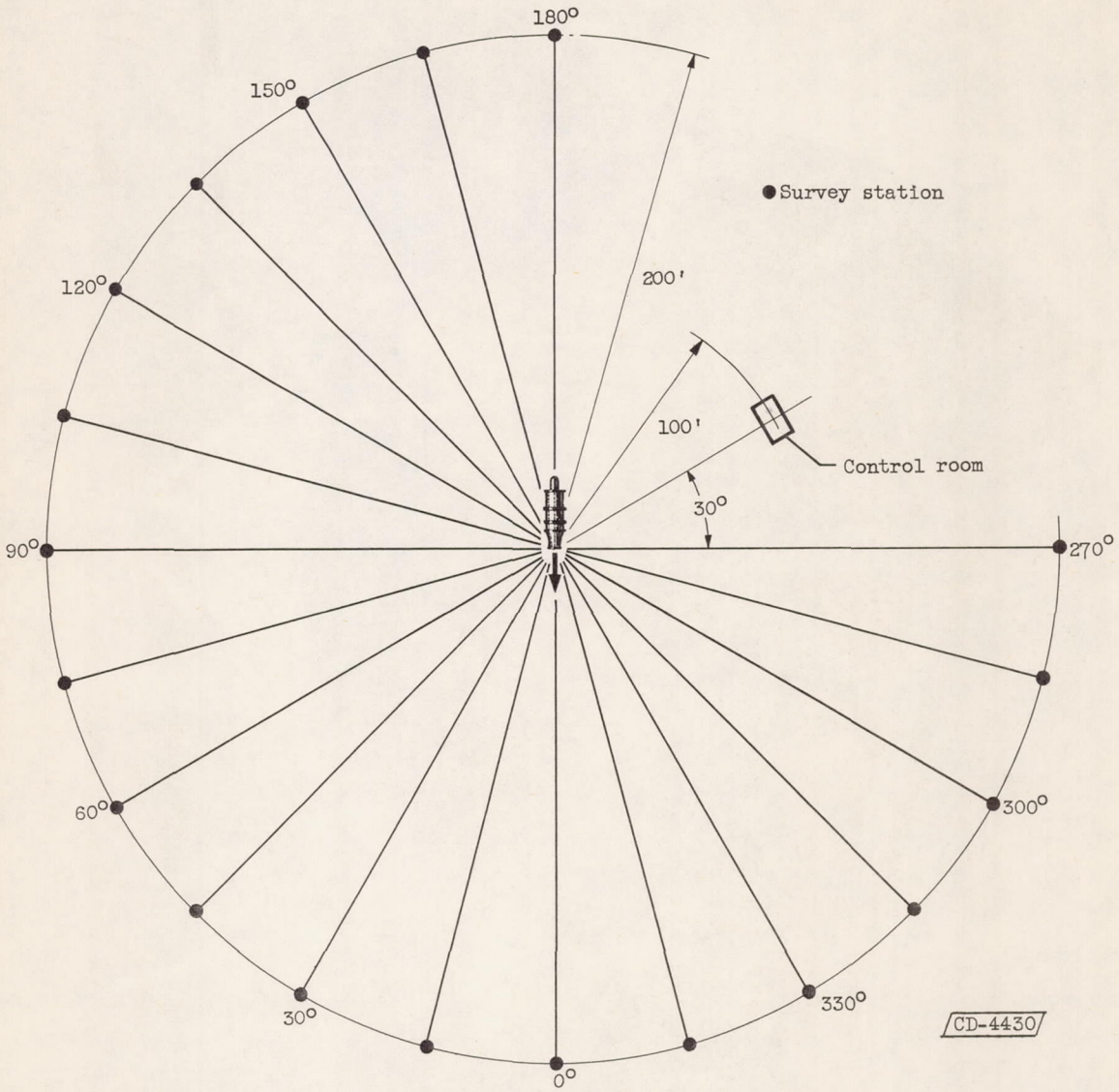

(b) Location of sound-survey stations and control room.

Figure 1. - Concluded. Free-field arrangement for noise surveys.

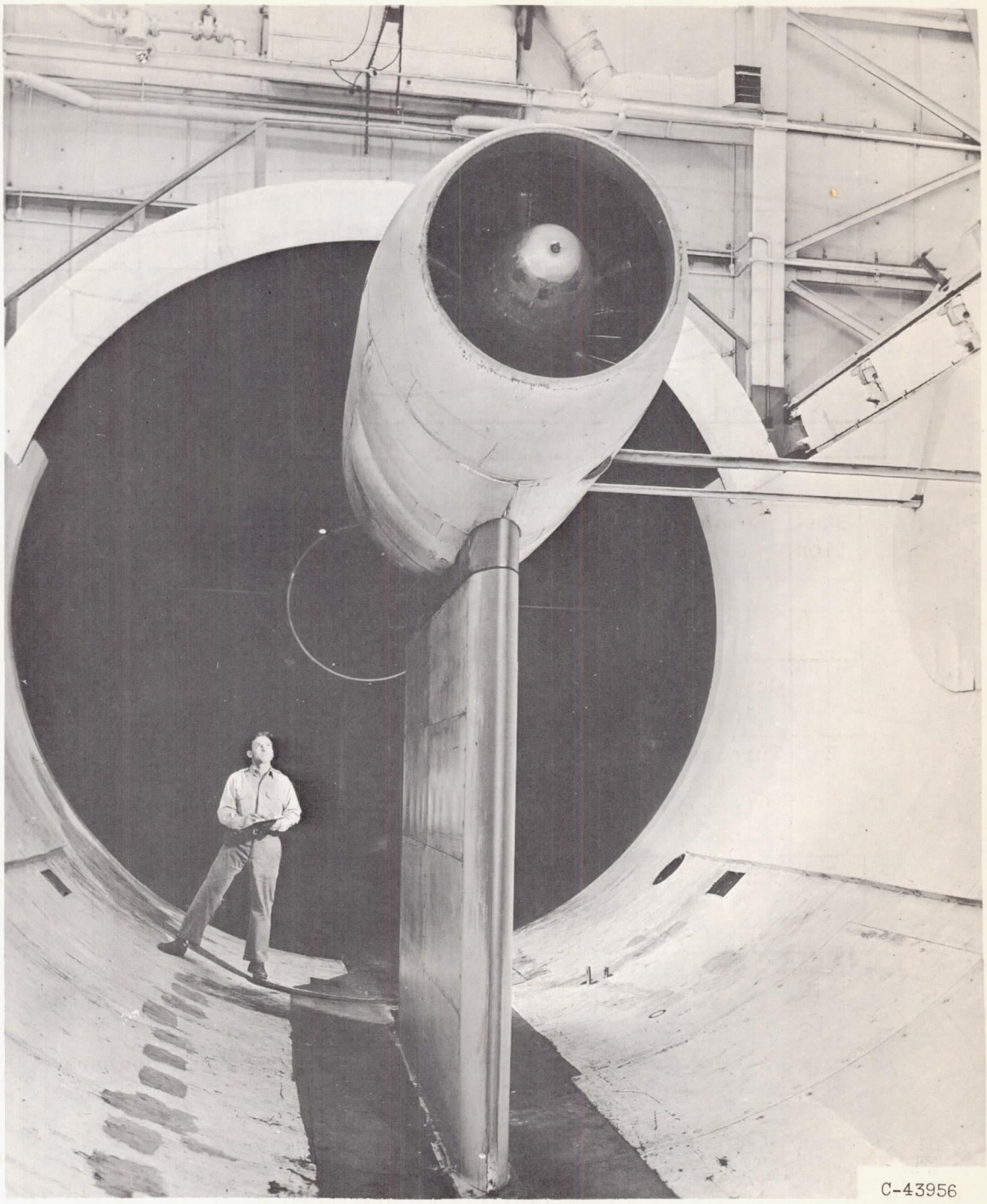

(a) Engine installed in tunnel.

Figure 2. - Installation and instrumentation of engine in altitude wind tunnel.

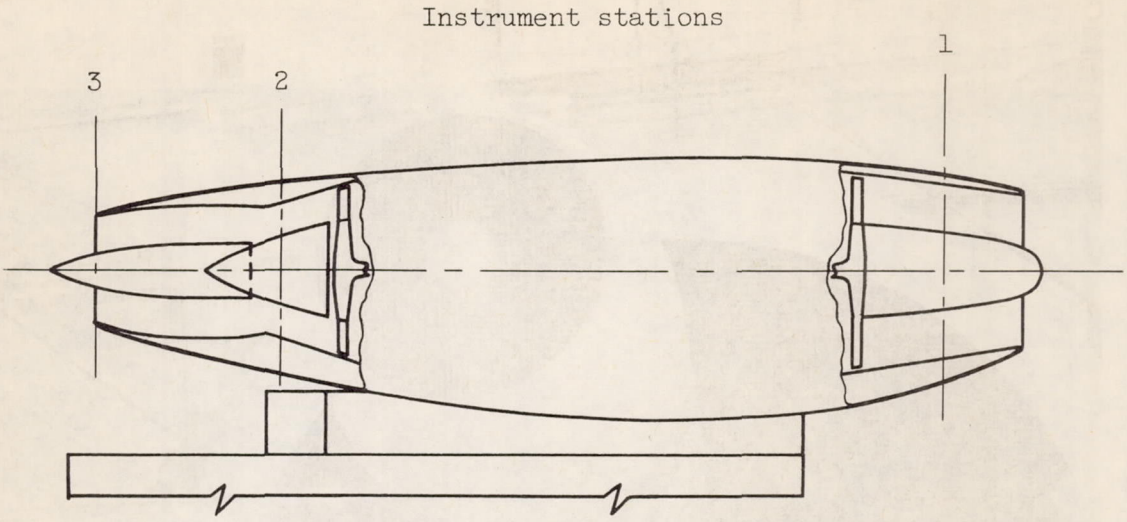

Station	Location	Total pressure		Total temperature		Static pressure	
		Probes	Rakes	Thermo-couples	Rakes	Probes	Rakes
1	Compressor inlet	40	4	16	4	[a]12	4
2	Turbine outlet (nozzle inlet)	24	4	24	4	--	-
3	Nozzle lip (external)	--	-	--	-	6	-

[a]Plus four outer-wall and four innerbody wall static-pressure taps.

Note: All rake instrumentation was located on the centers of equal areas.

(b) Engine instrumentation.

Figure 2. - Concluded. Installation and instrumentation of engine in altitude wind tunnel.

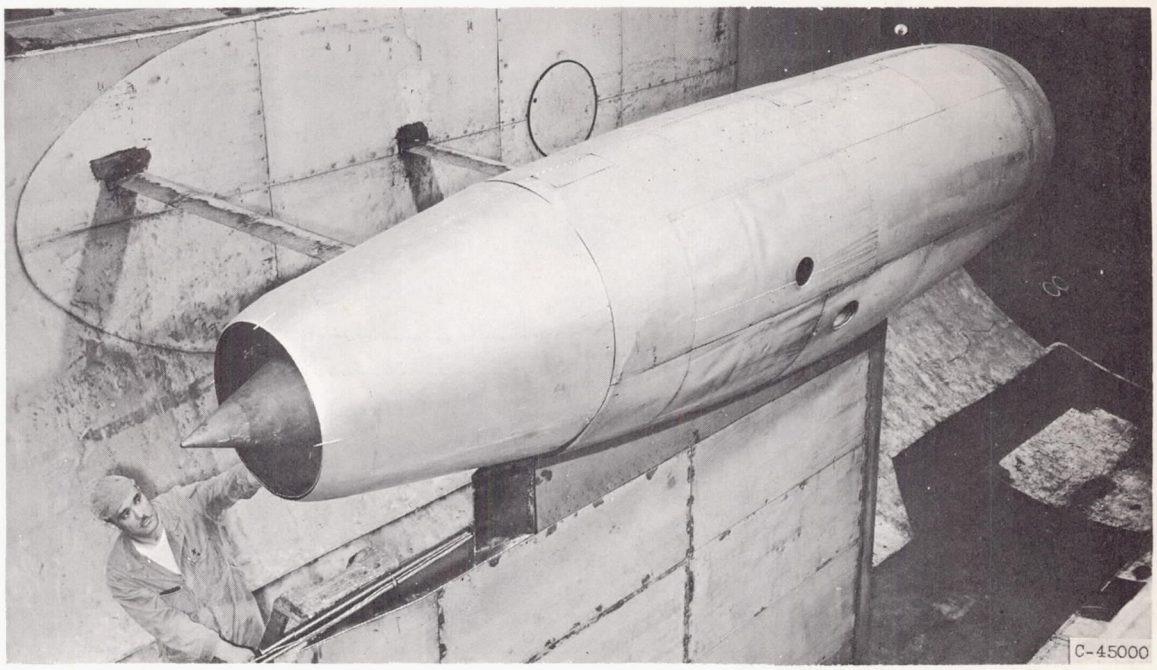

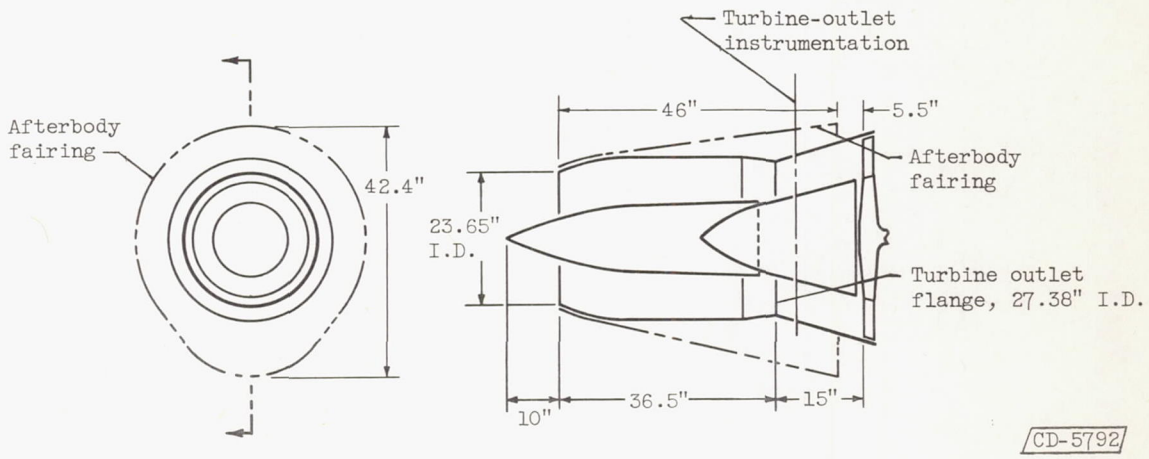

Figure 3. - Standard nozzle.

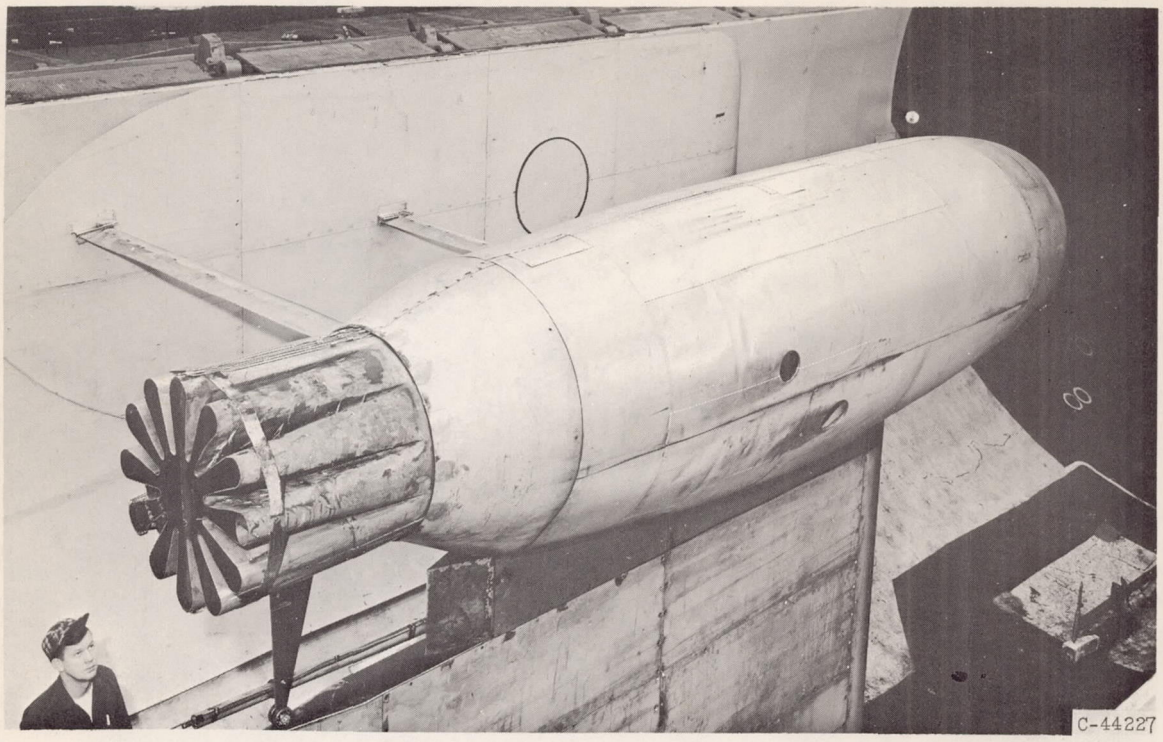

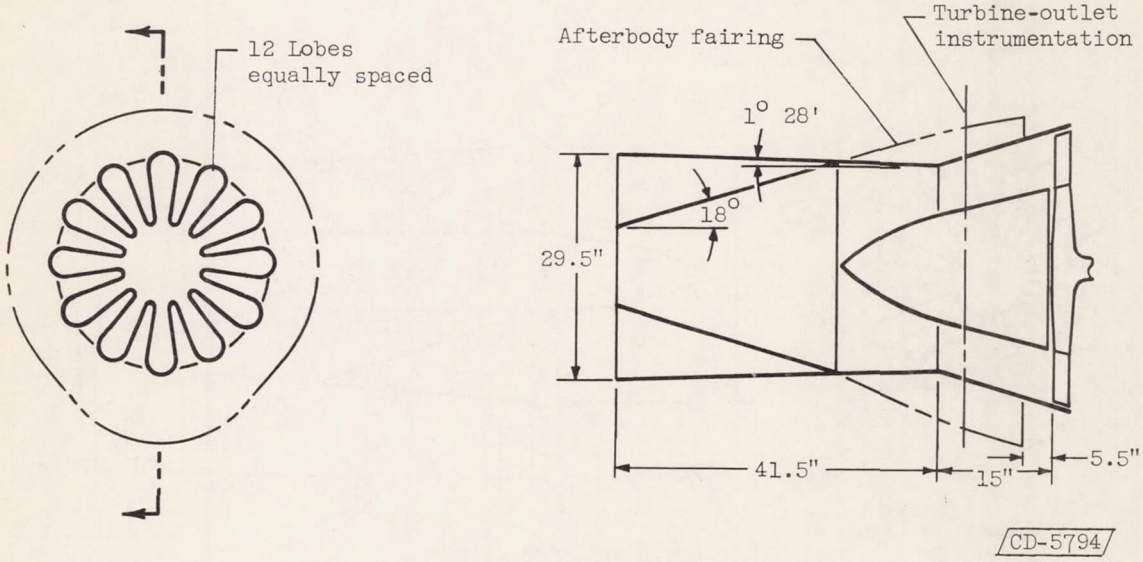

(a) 12-Lobe nozzle.

Figure 4. - Noise-suppressor configurations.

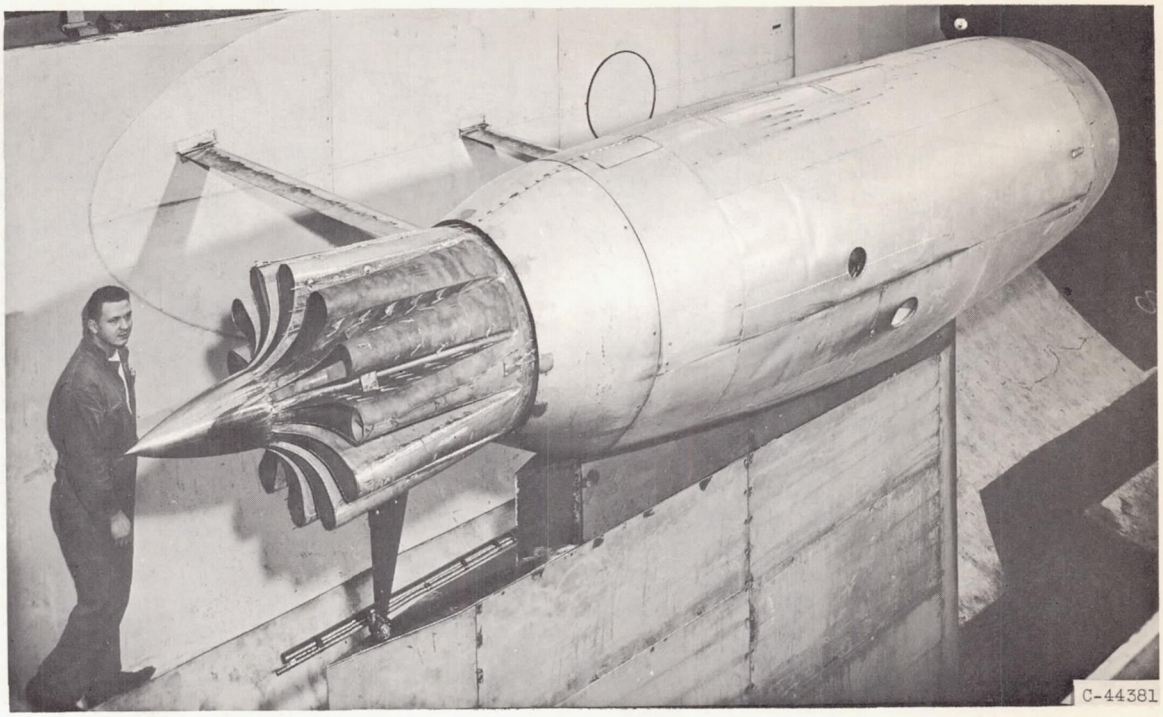

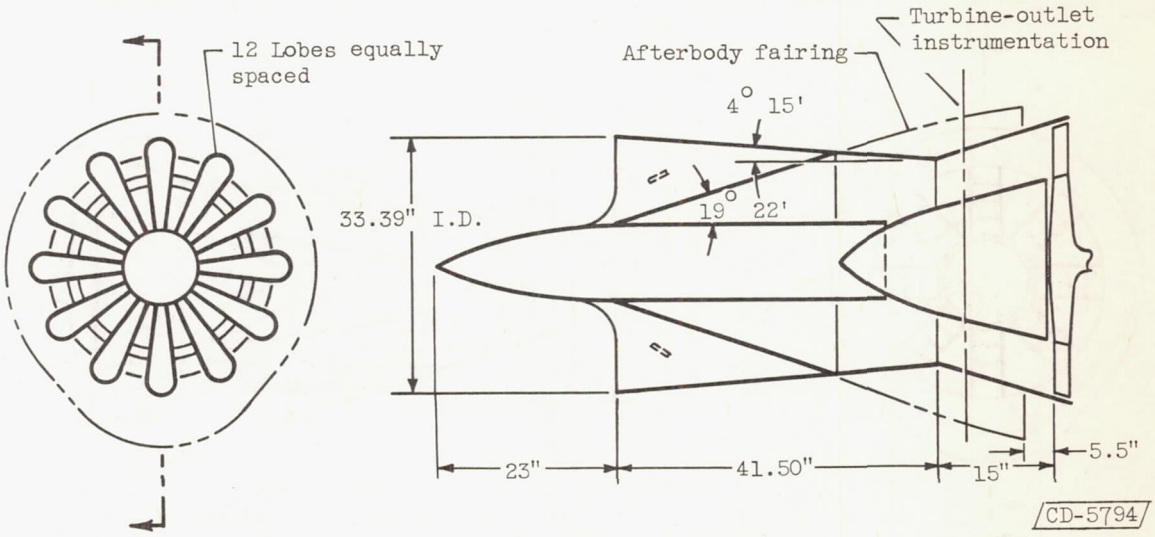

(b) 12-Lobe nozzle with centerbody.

Figure 4. - Continued. Noise-suppressor configurations.

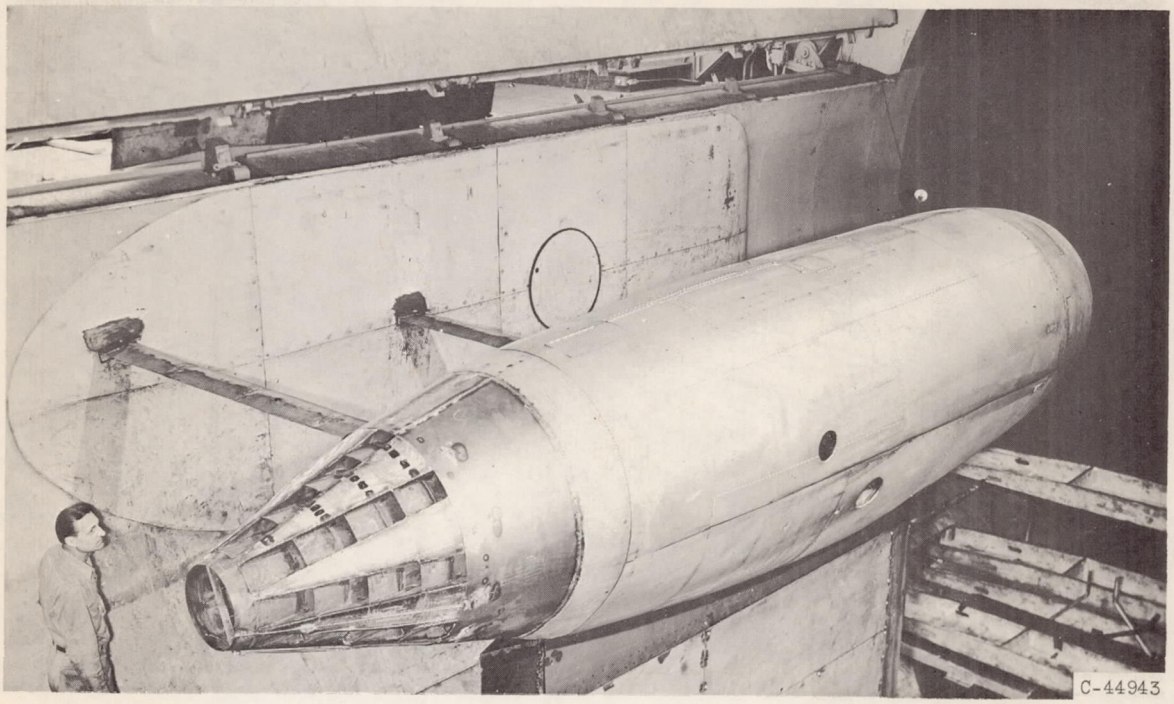

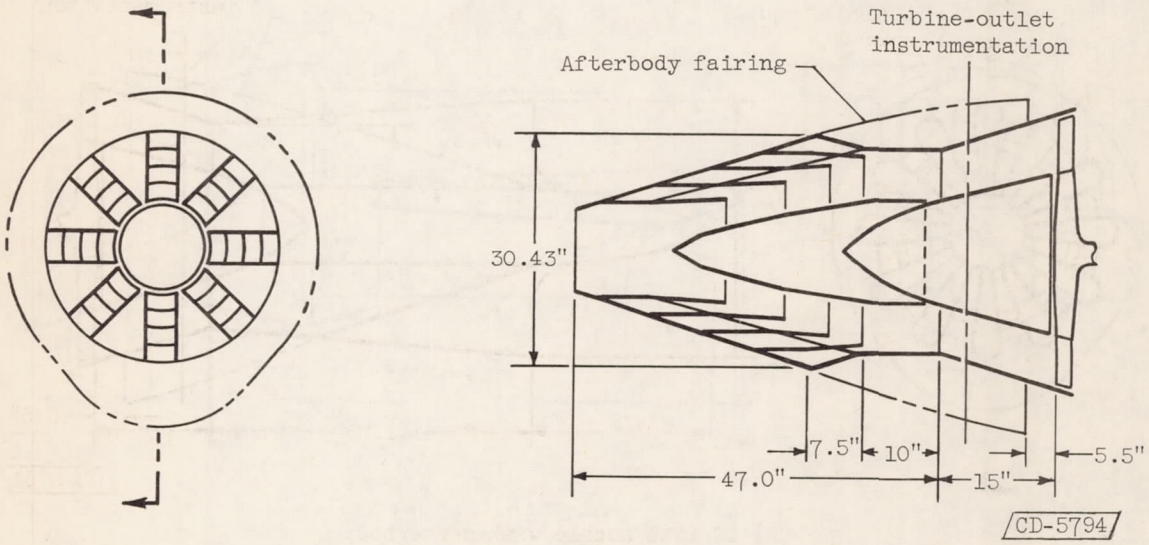

(c) Segmented-lobe nozzle.

Figure 4. - Continued. Noise-suppressor configurations.

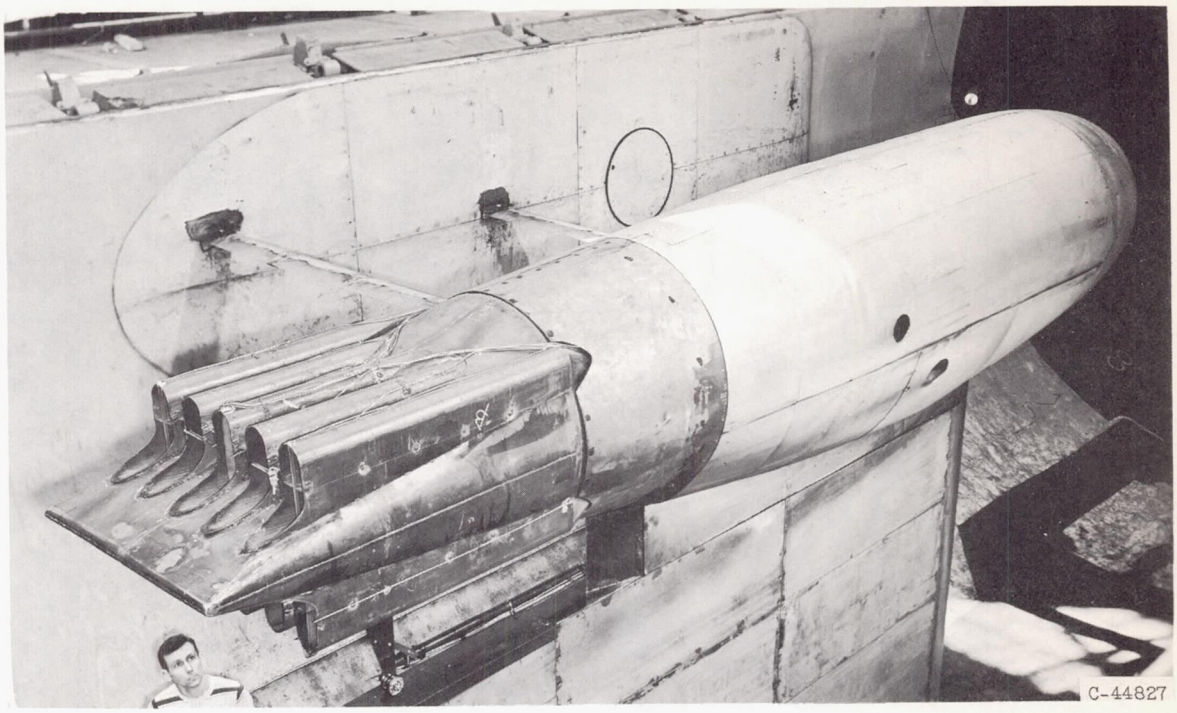

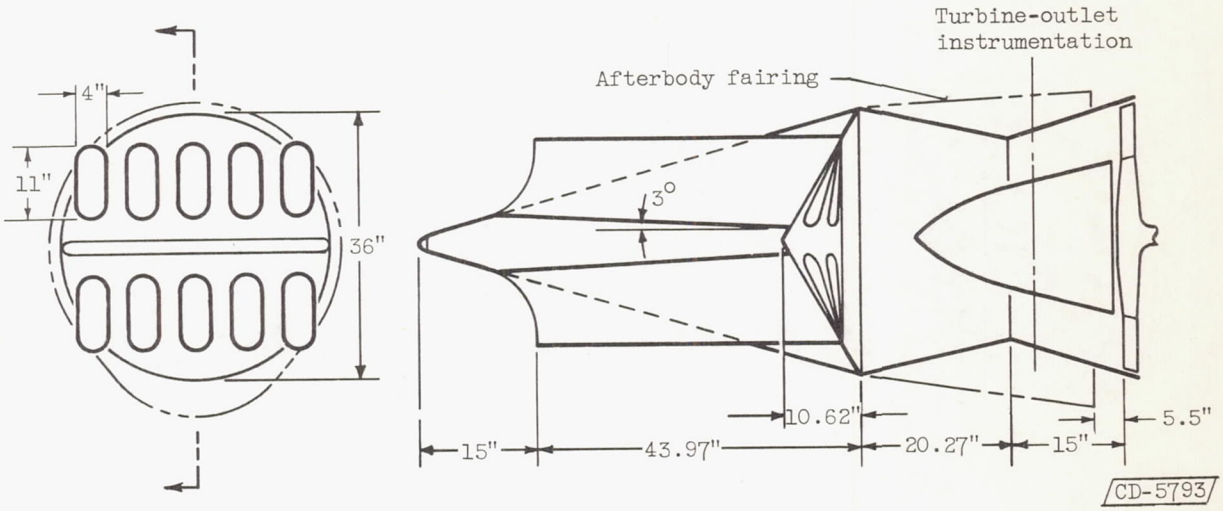

(d) 10-Tube nozzle, rectangular exits.

Figure 4. - Continued. Noise-suppressor configurations.

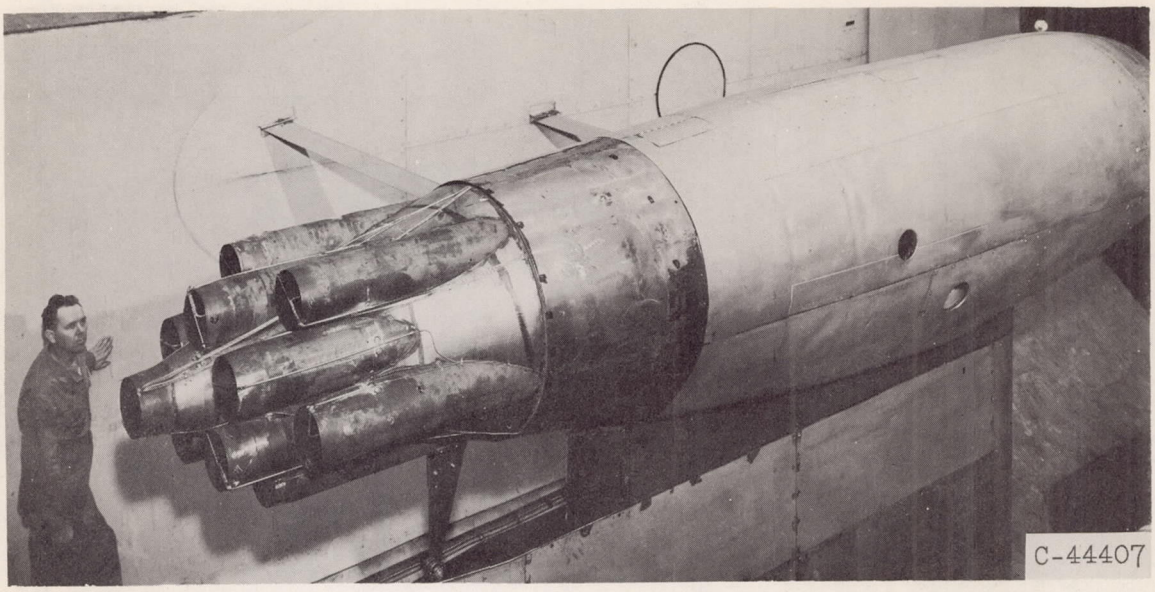

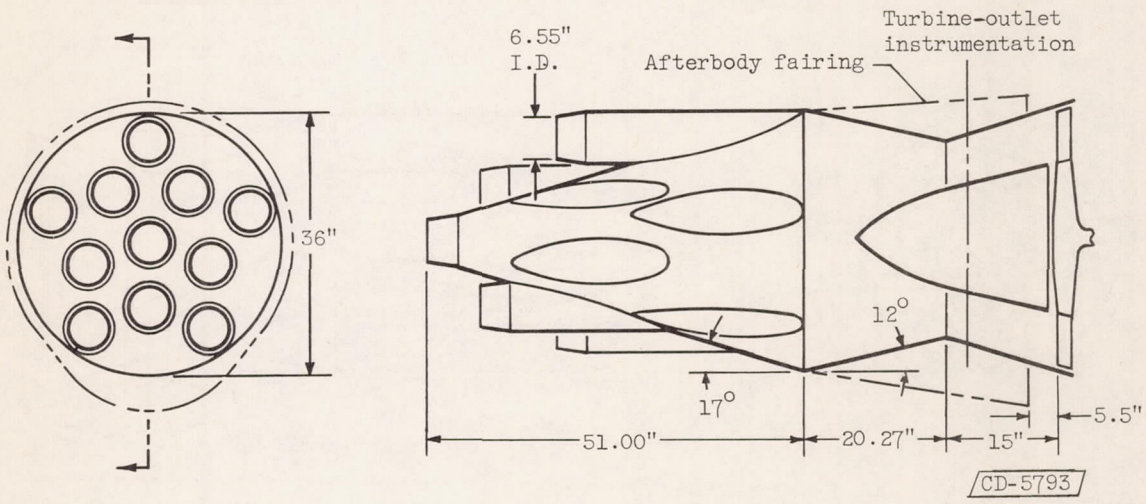

(e) 11-Tube nozzle, circular exits.

Figure 4. - Continued. Noise-suppressor configurations.

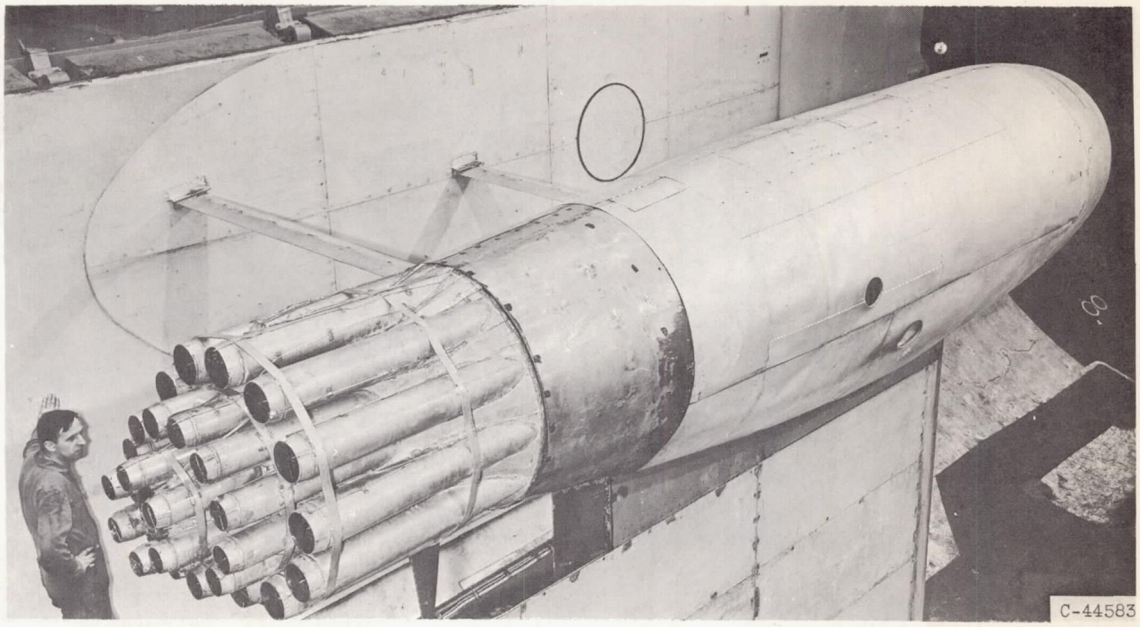

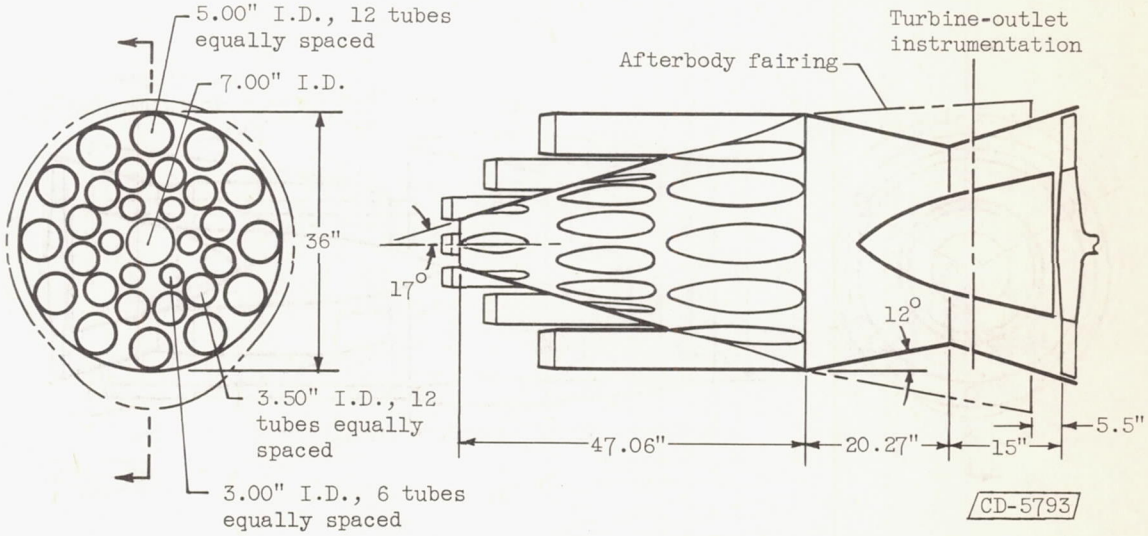

(f) 31-Tube nozzle, circular exits.

Figure 4. Continued. Noise-suppressor configurations.

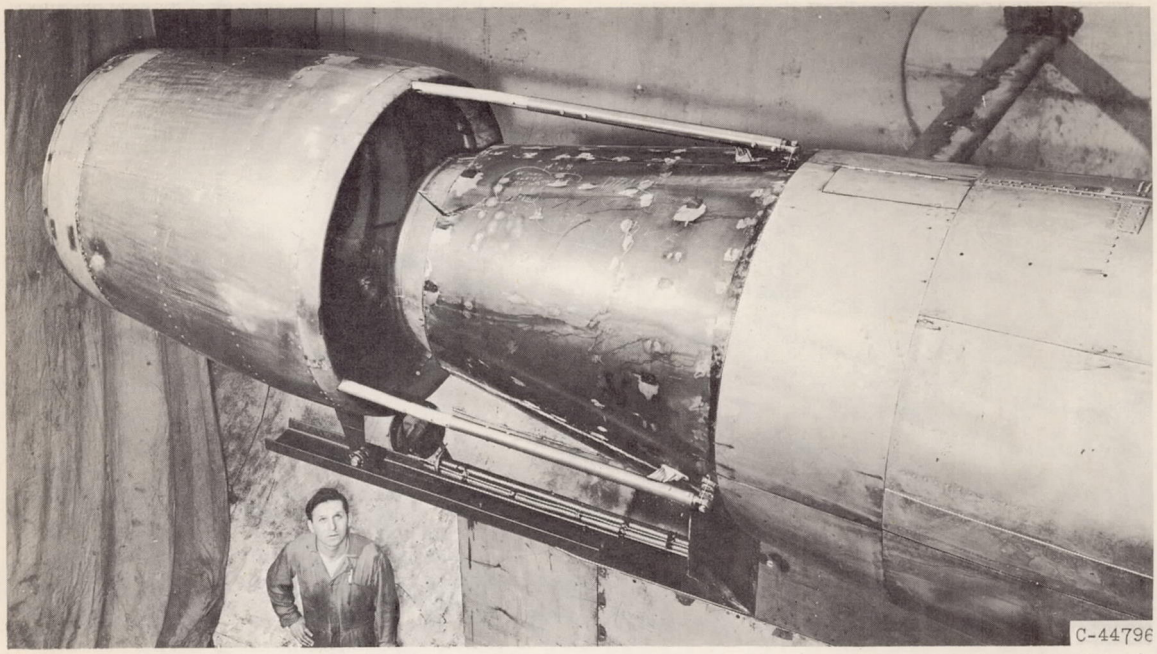

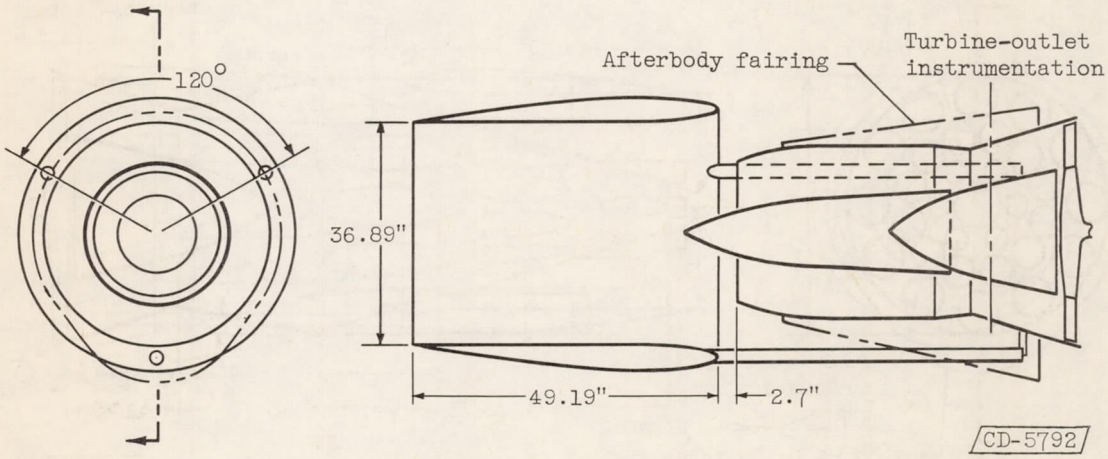

(g) Standard nozzle with ejector.

Figure 4. - Continued. Noise-suppressor configurations.

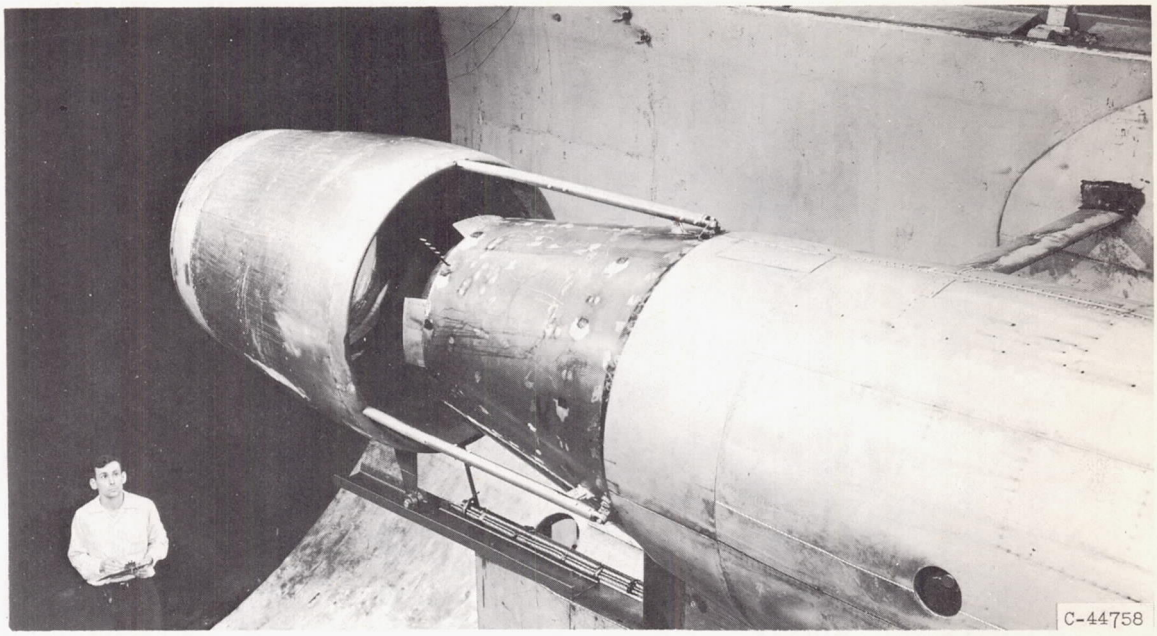

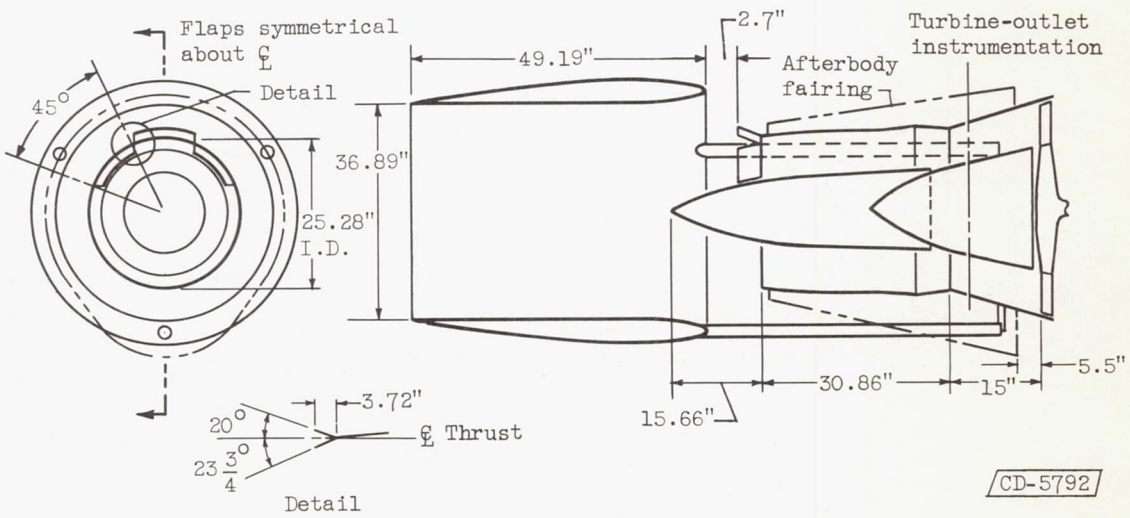

(h) Mixing nozzle with ejector.

Figure 4. - Concluded. Noise-suppressor configurations.

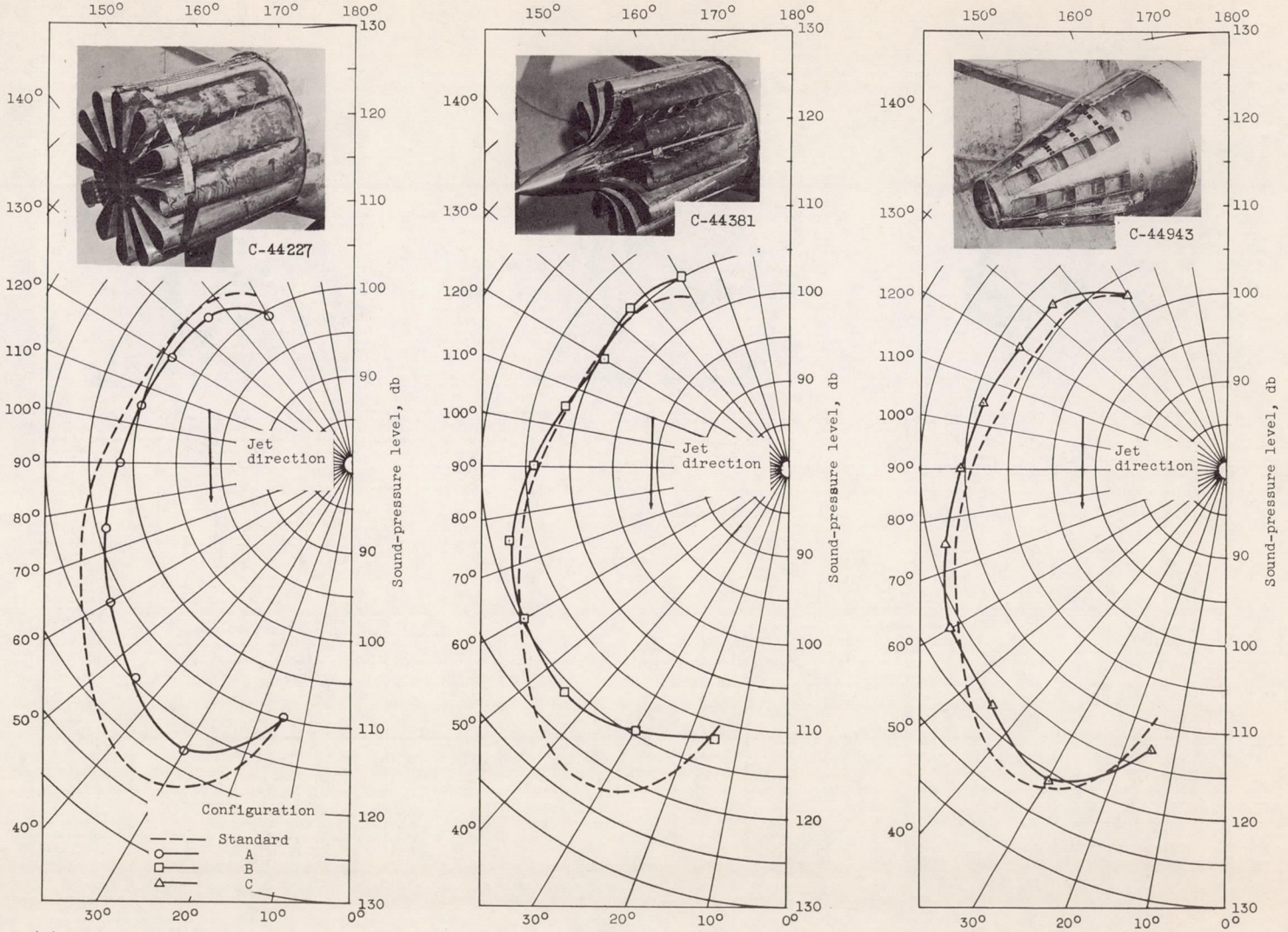

(a) 12-Lobe nozzle (configuration A).

(b) 12-Lobe nozzle with centerbody (configuration B).

(c) Segmented-lobe nozzle (configuration C).

Figure 5. - Polar sound-pressure levels of lobe-type nozzles.

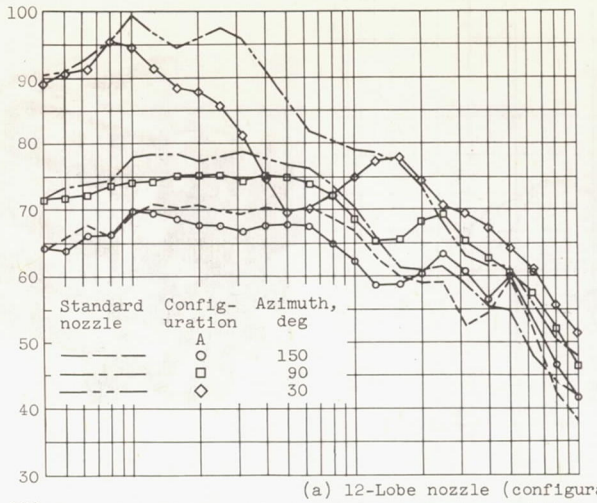

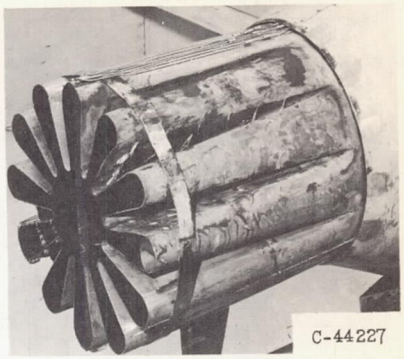

(a) 12-Lobe nozzle (configuration A).

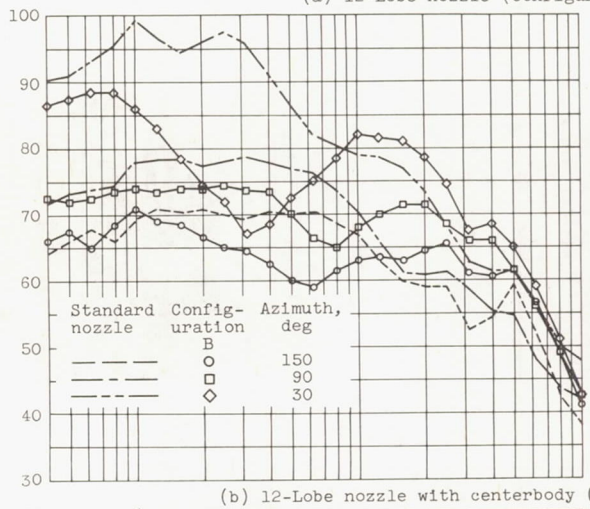

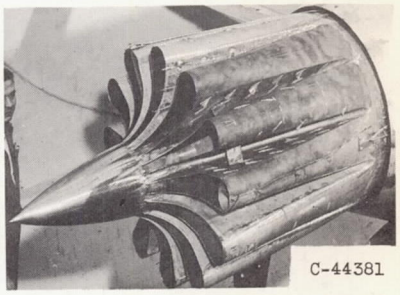

(b) 12-Lobe nozzle with centerbody (configuration B).

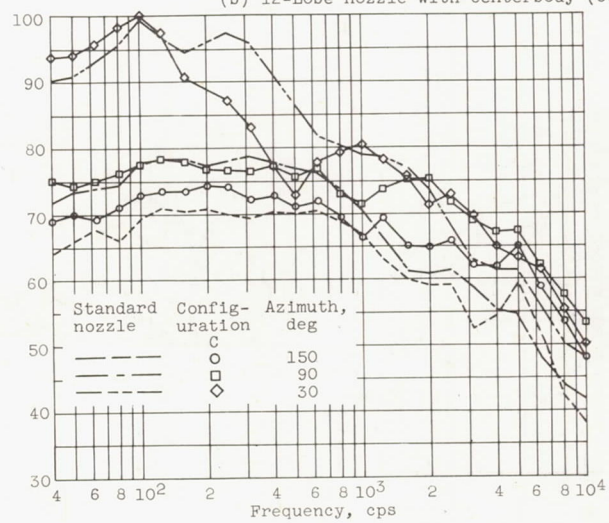

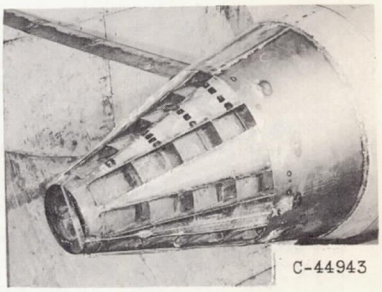

(c) Segmented-lobe nozzle (configuration C).

Figure 6. - Spectrum levels of lobe-type nozzles.

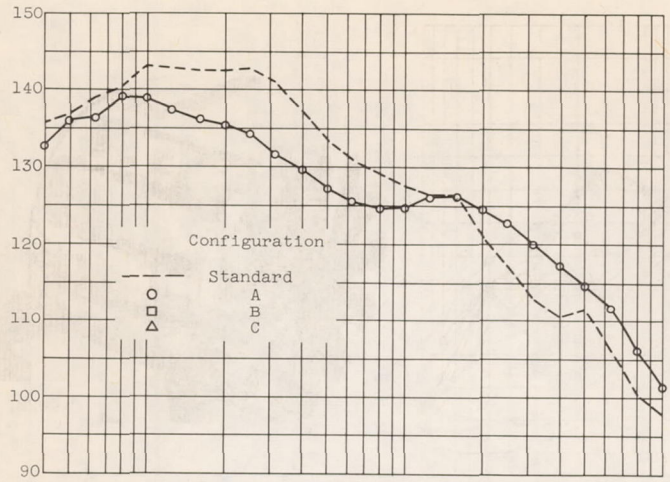

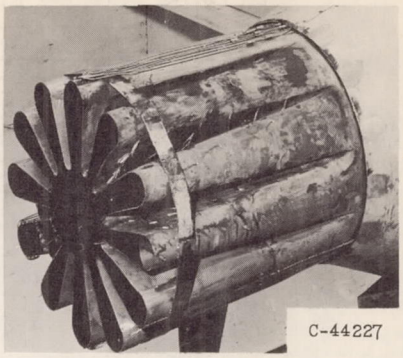

(a) 12-Lobe nozzle (configuration A).

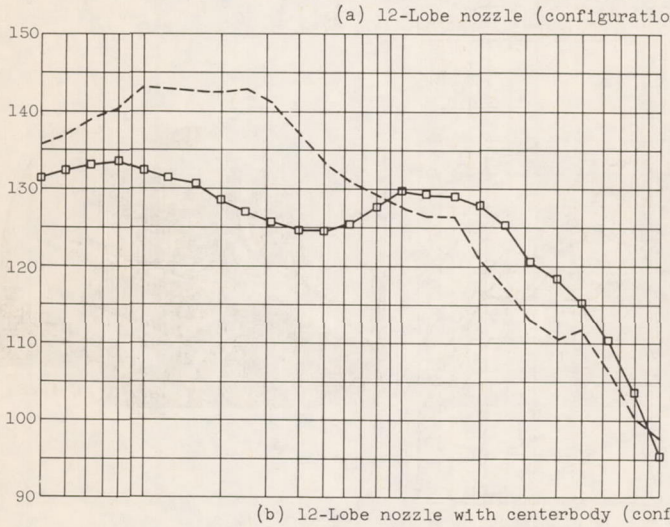

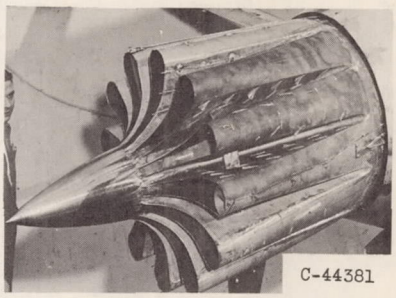

(b) 12-Lobe nozzle with centerbody (configuration B).

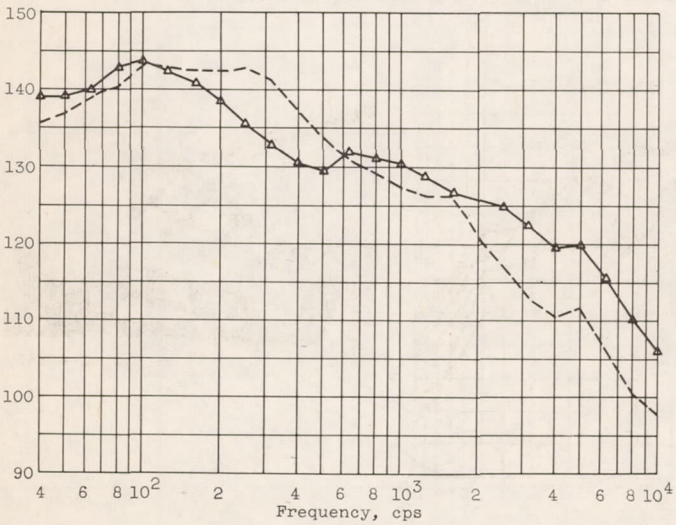

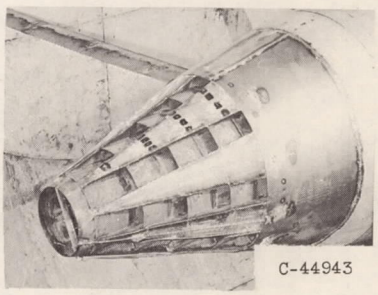

(c) Segmented-lobe nozzle (configuration C).

Figure 7. - Frequency distribution of power-spectrum levels of lobe-type nozzles.

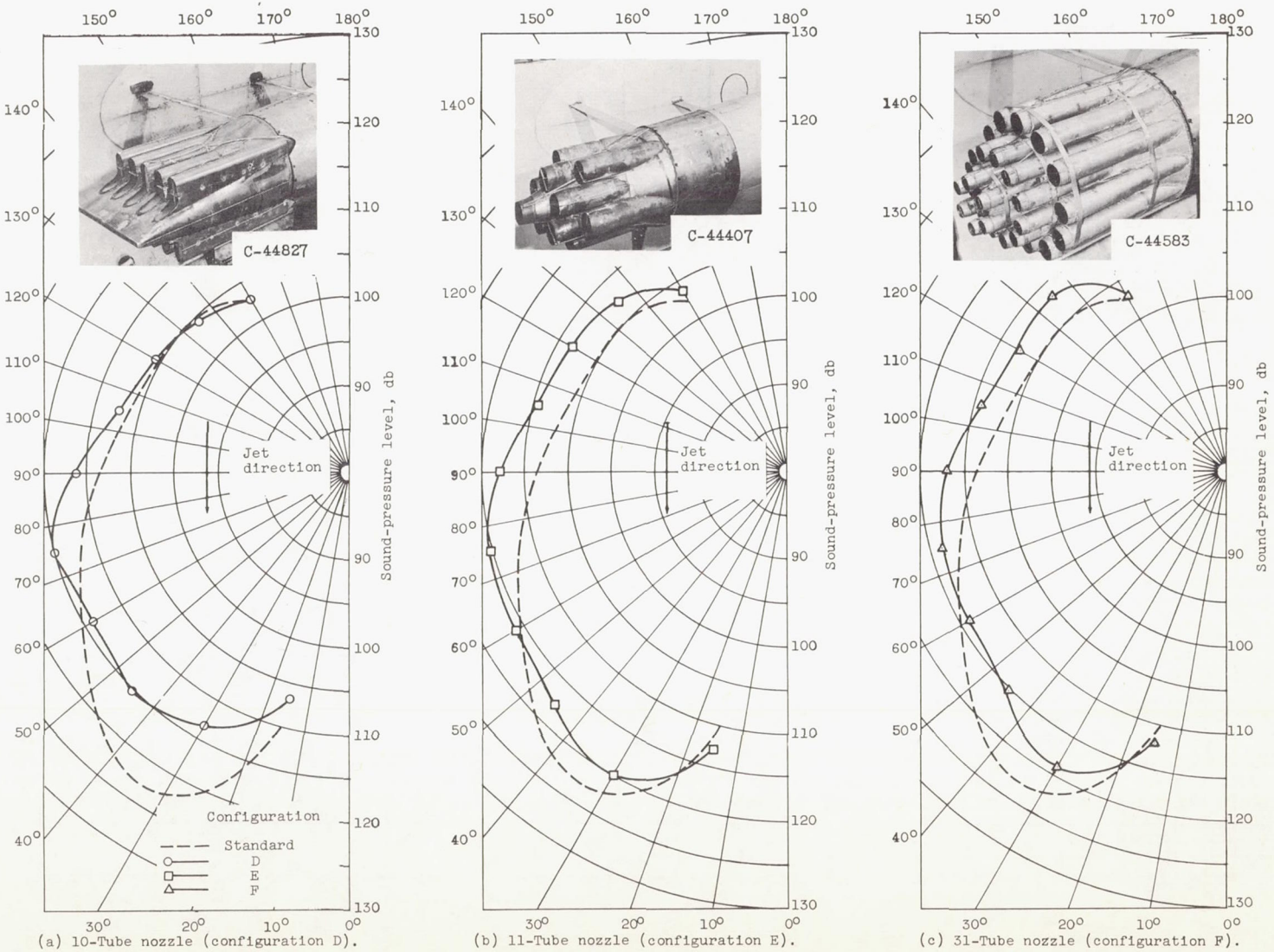

(a) 10-Tube nozzle (configuration D).

(b) 11-Tube nozzle (configuration E).

(c) 31-Tube nozzle (configuration F).

Figure 8. - Polar sound-pressure levels of tube-type nozzles.

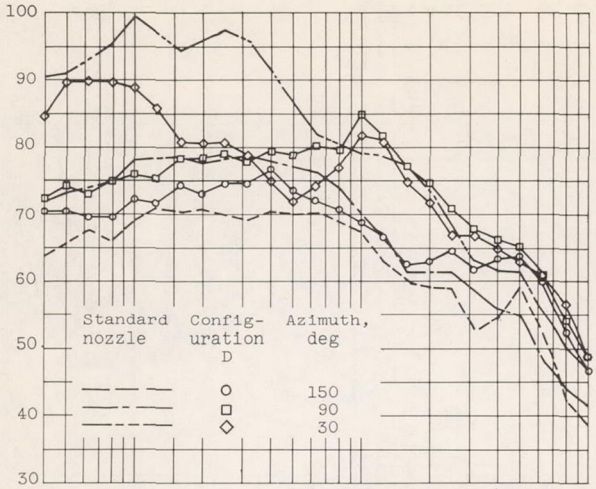

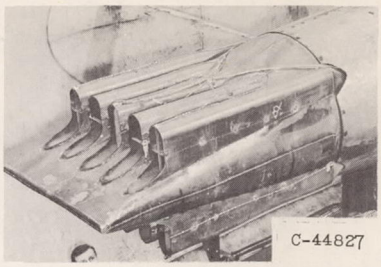

(a) 10-Tube nozzle (configuration D).

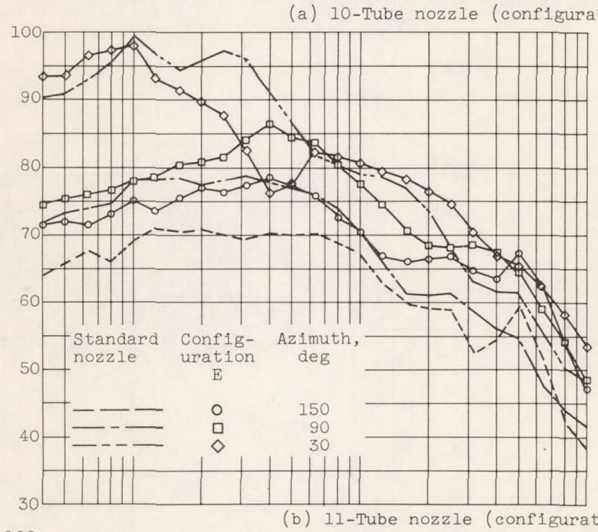

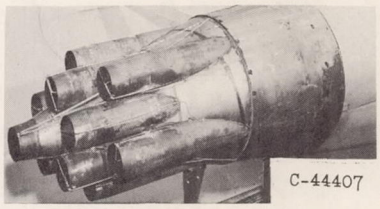

(b) 11-Tube nozzle (configuration E).

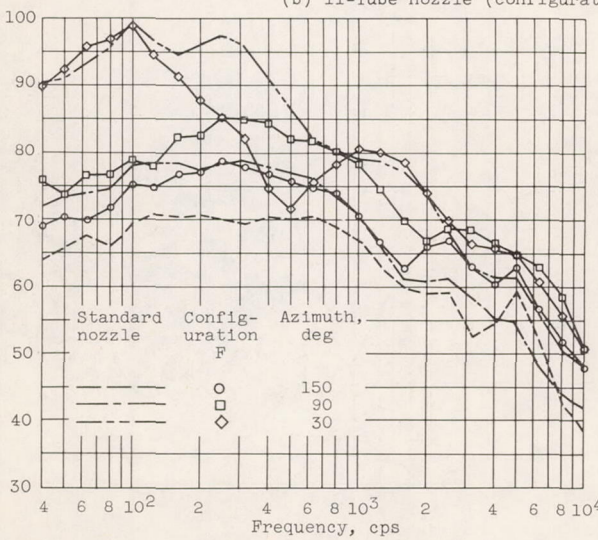

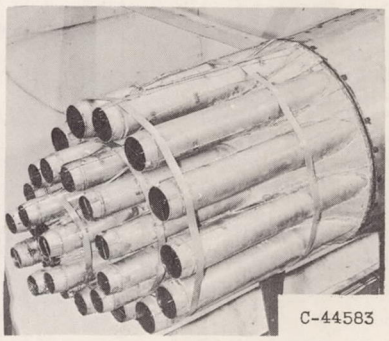

(c) 31-Tube nozzle (configuration F).

Figure 9. - Spectrum levels of tube-type nozzles.

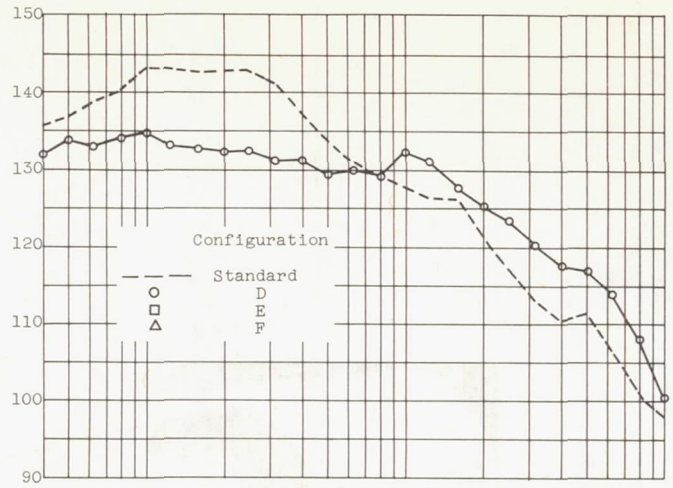

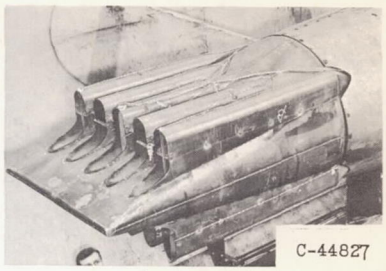

(a) 10-Tube nozzle (configuration D).

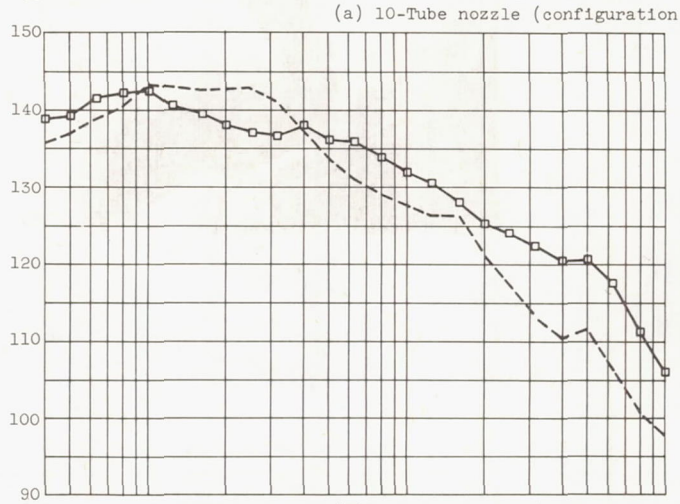

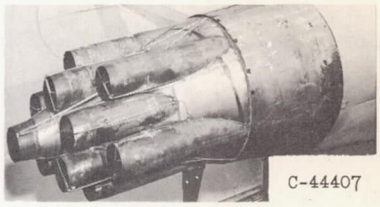

(b) 11-Tube nozzle (configuration E).

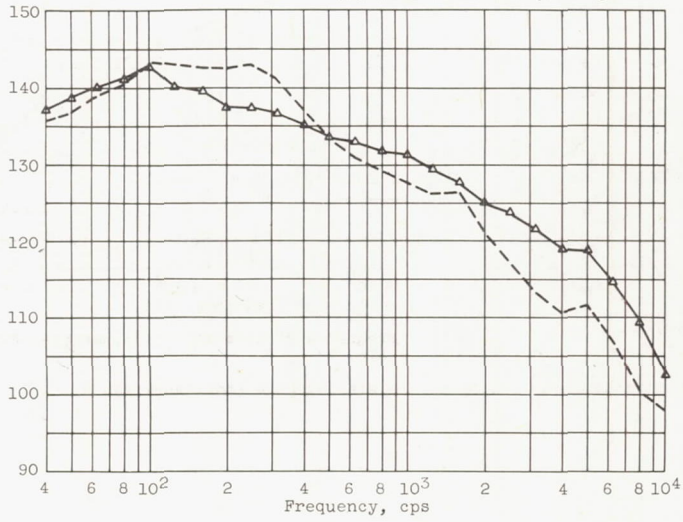

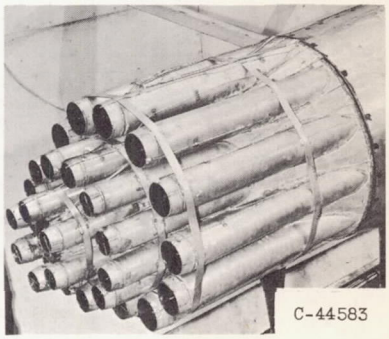

(c) 31-Tube nozzle (configuration F).

Figure 10. - Frequency distribution of power-spectrum levels for tube-type nozzles.

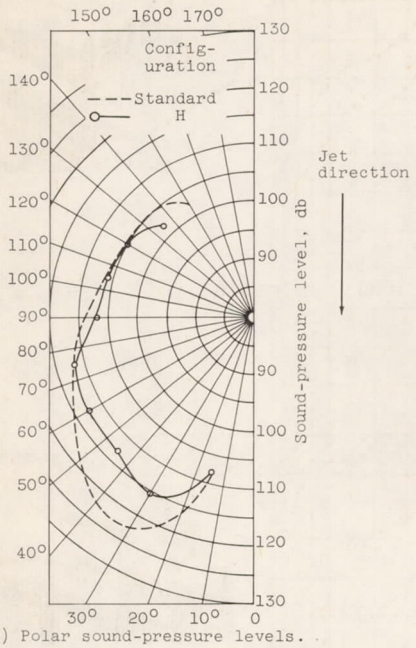

(a) Polar sound-pressure levels.

Jet direction

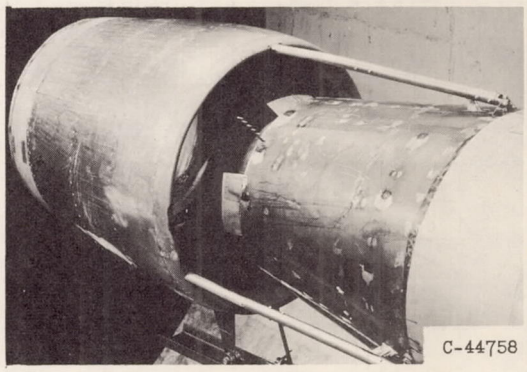

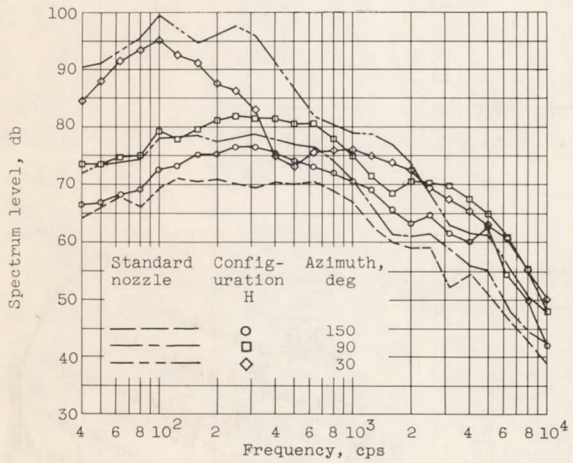

(b) Spectrum levels.

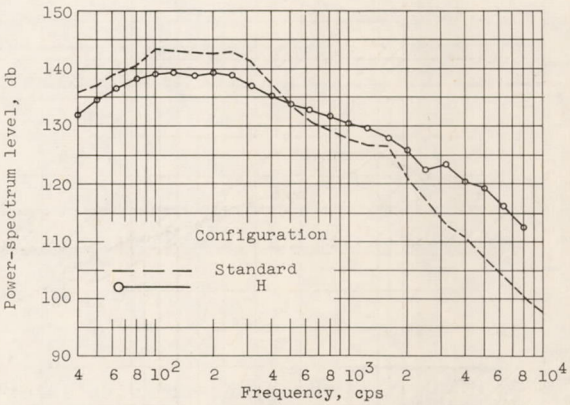

(c) Frequency distribution of power-spectrum levels.

Figure 11. - Acoustic characteristics of mixing nozzle with ejector (configuration H).

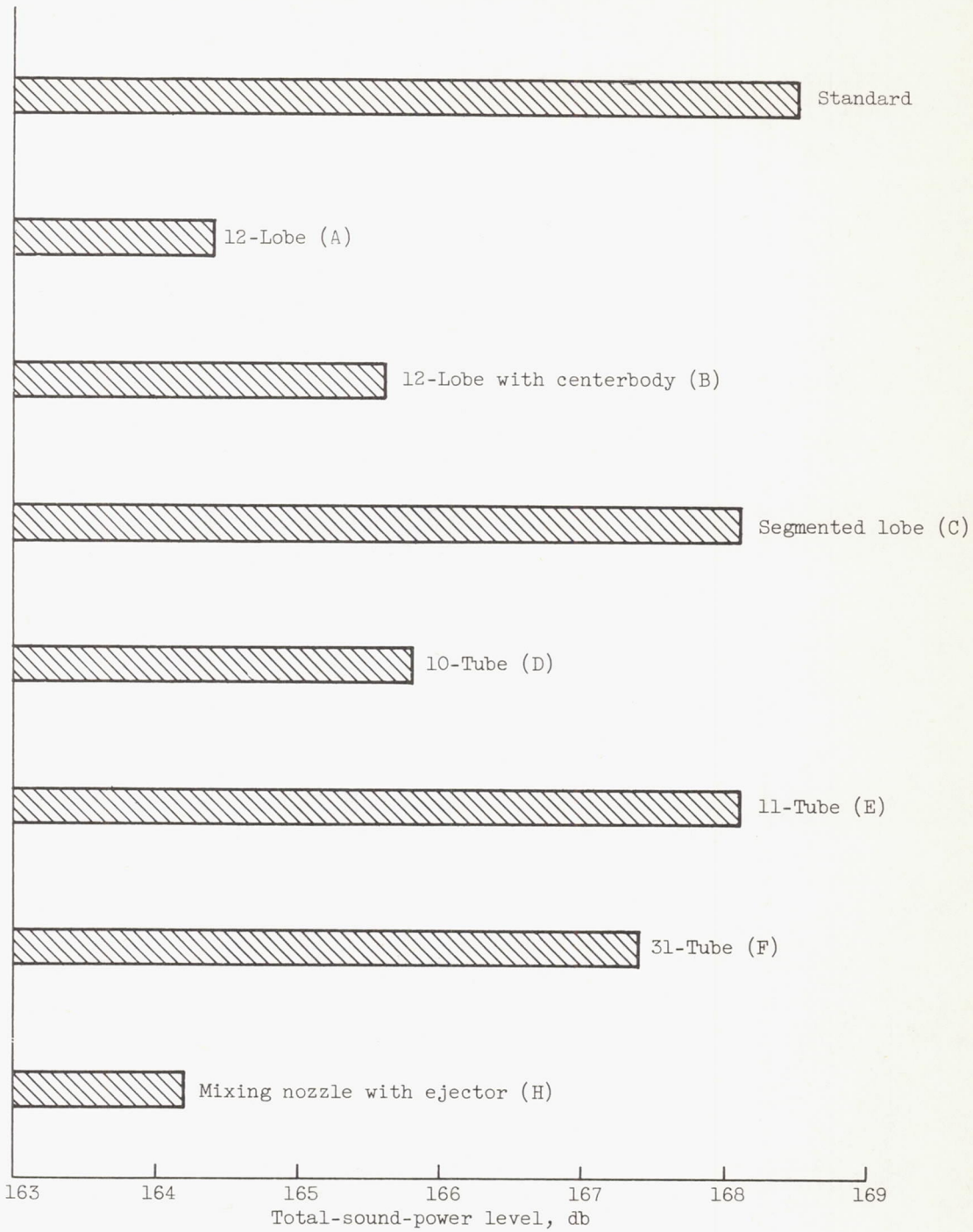

Figure 12. - Comparison of total sound-power.

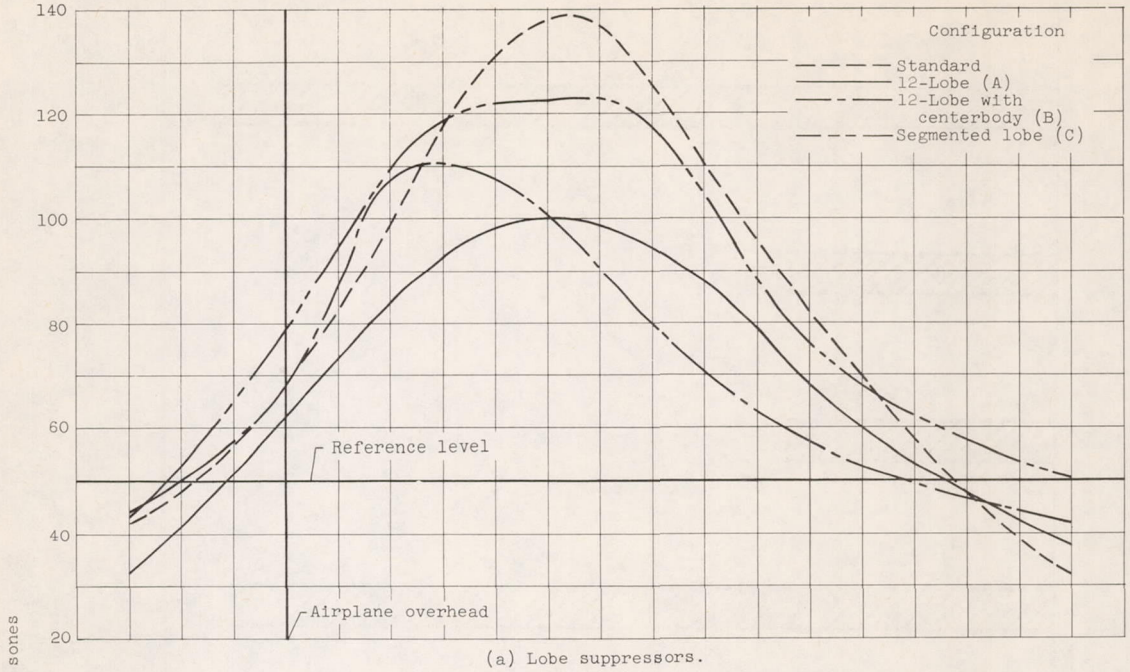

(a) Lobe suppressors.

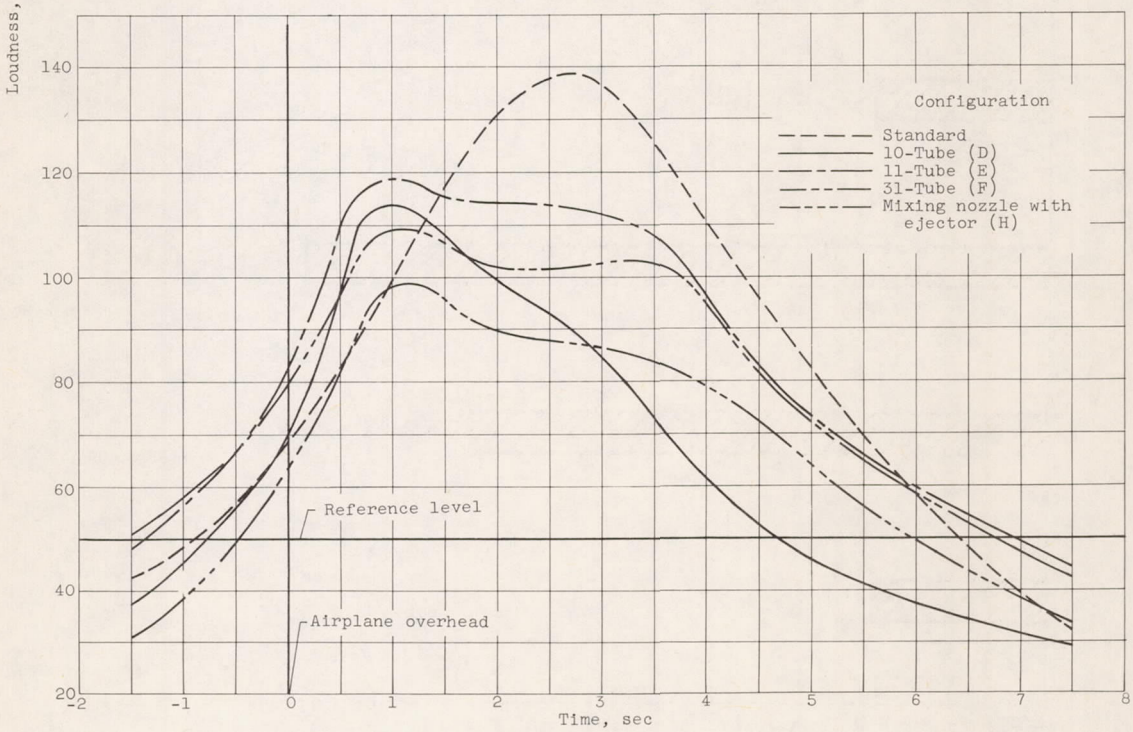

(b) Tube and ejector suppressors.

Figure 13. - Calculated time history of jet loudness as heard by ground observer.

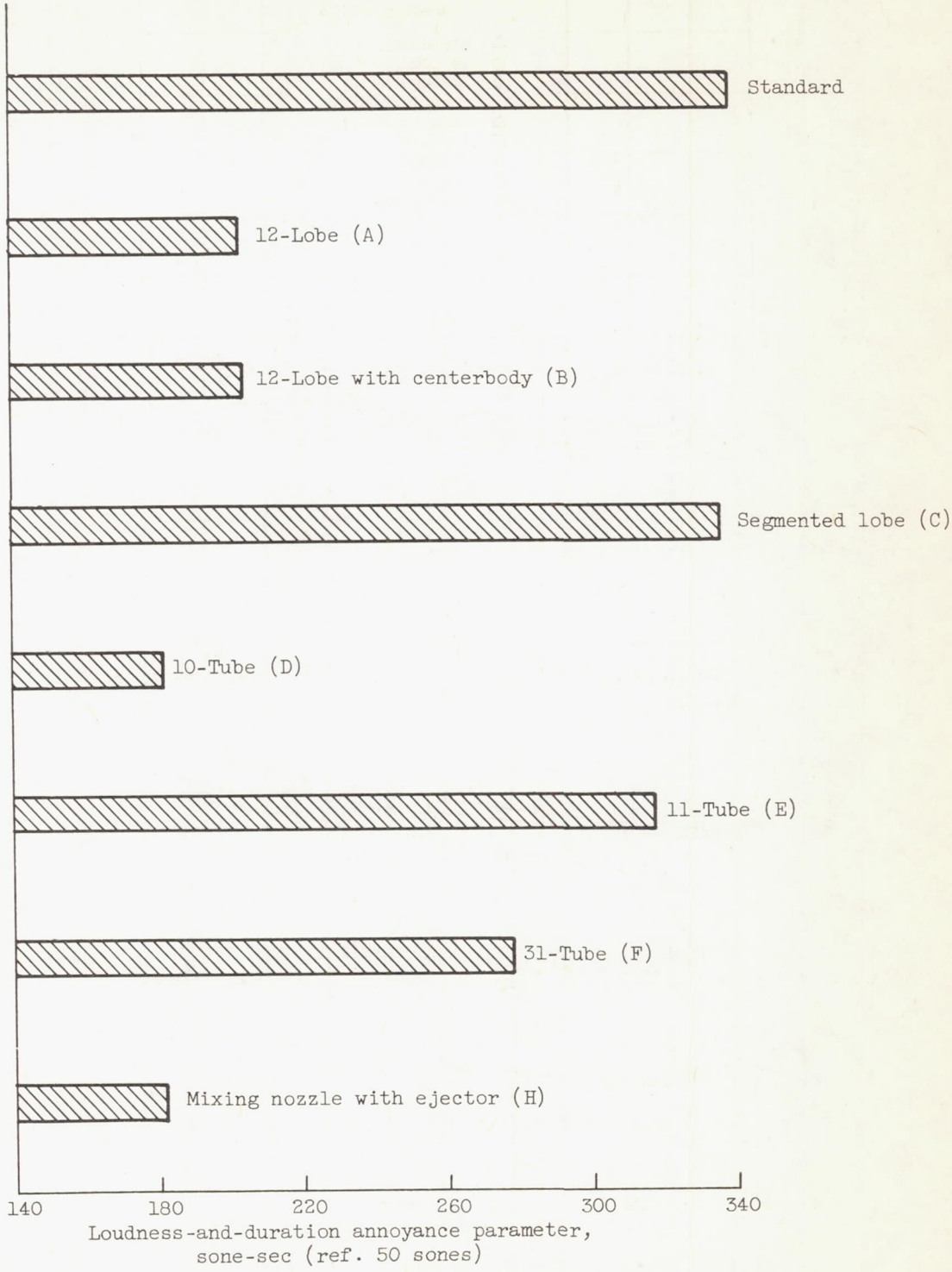

Figure 14. - Comparison of noise loudness and duration.

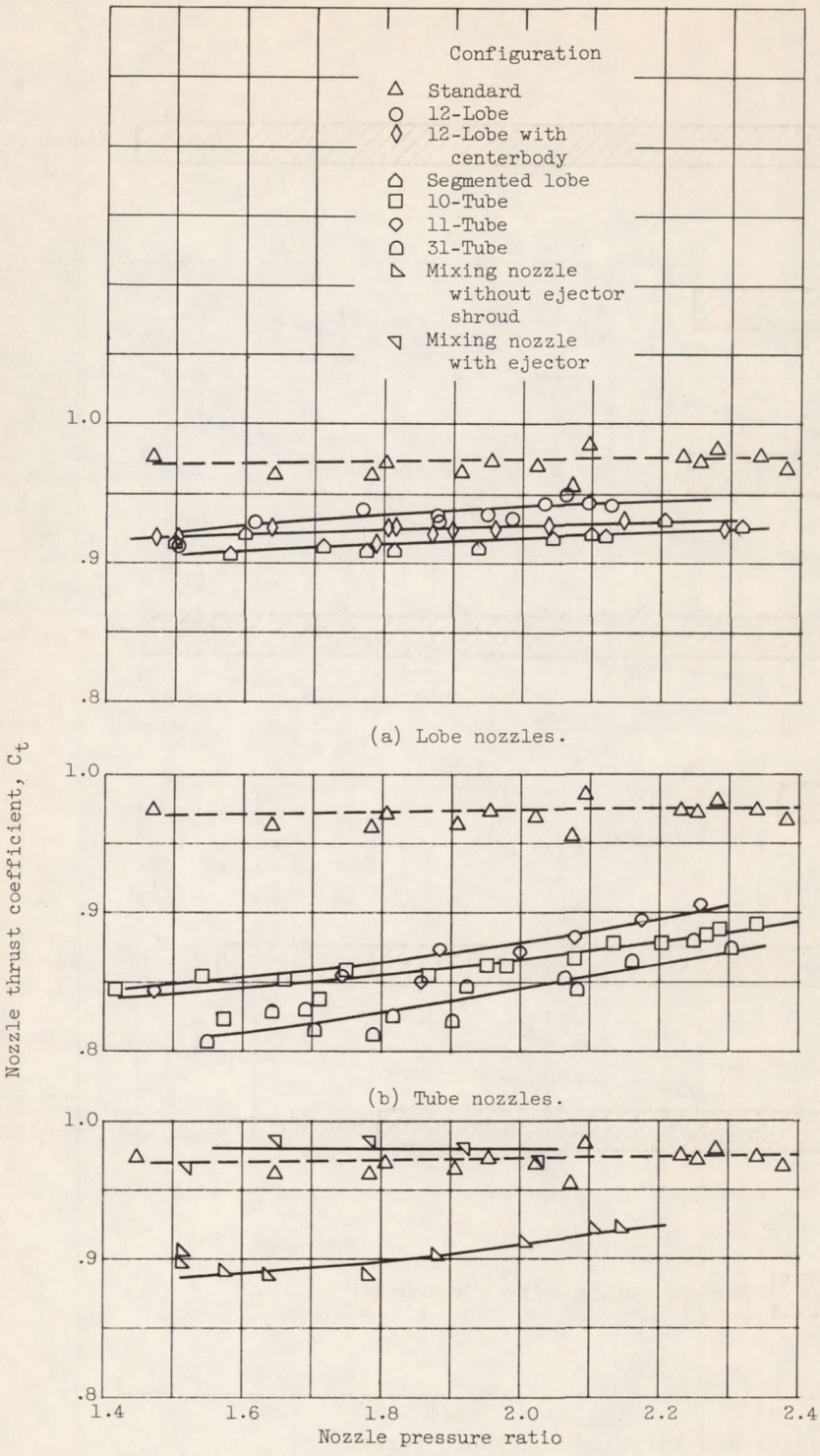

(a) Lobe nozzles.

(b) Tube nozzles.

(c) Mixing nozzles.

Figure 15. - Comparison of thrust coefficients of noise-suppression nozzles and standard nozzle.

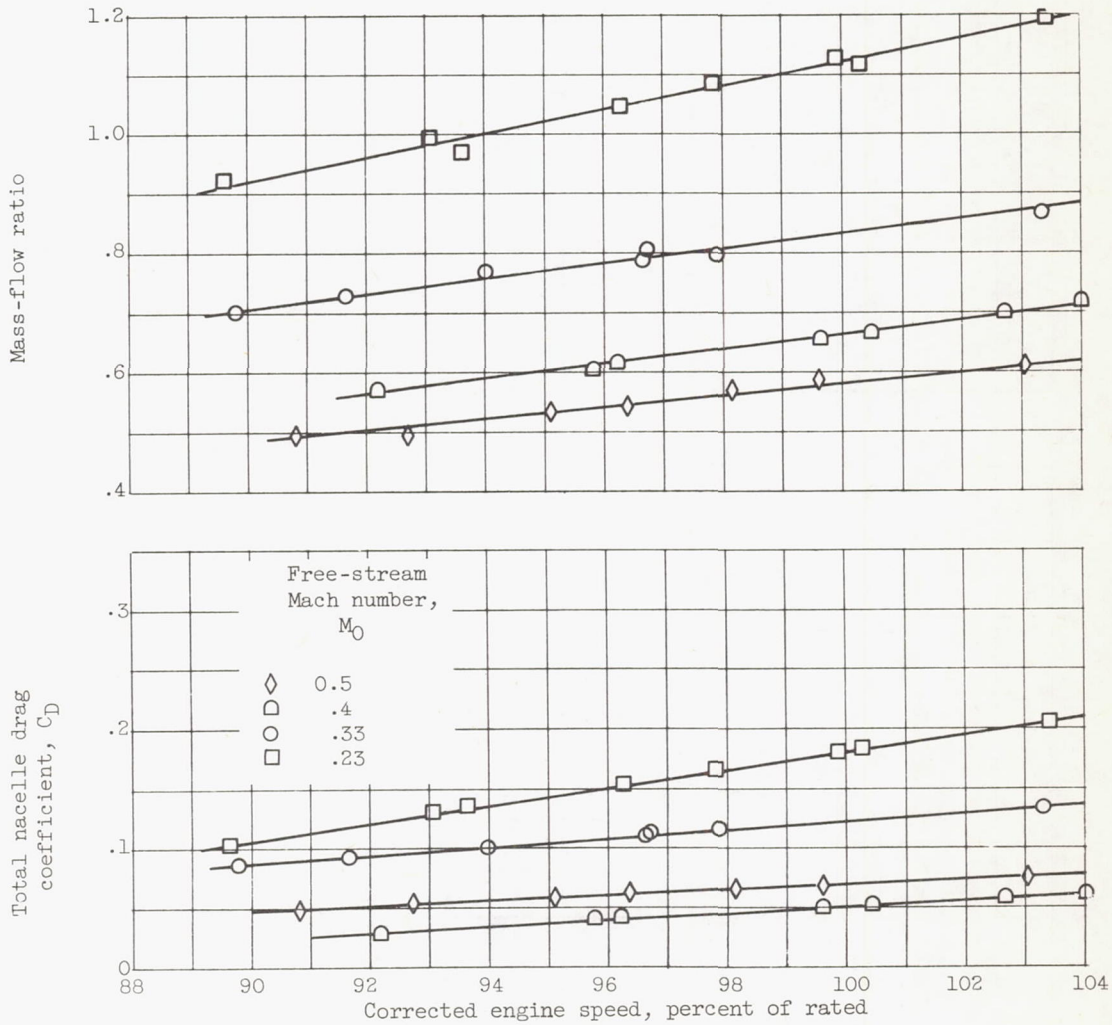

Figure 16. - Variation of engine mass-flow ratio and total nacelle drag coefficient with engine speed and Mach number for standard nozzle.

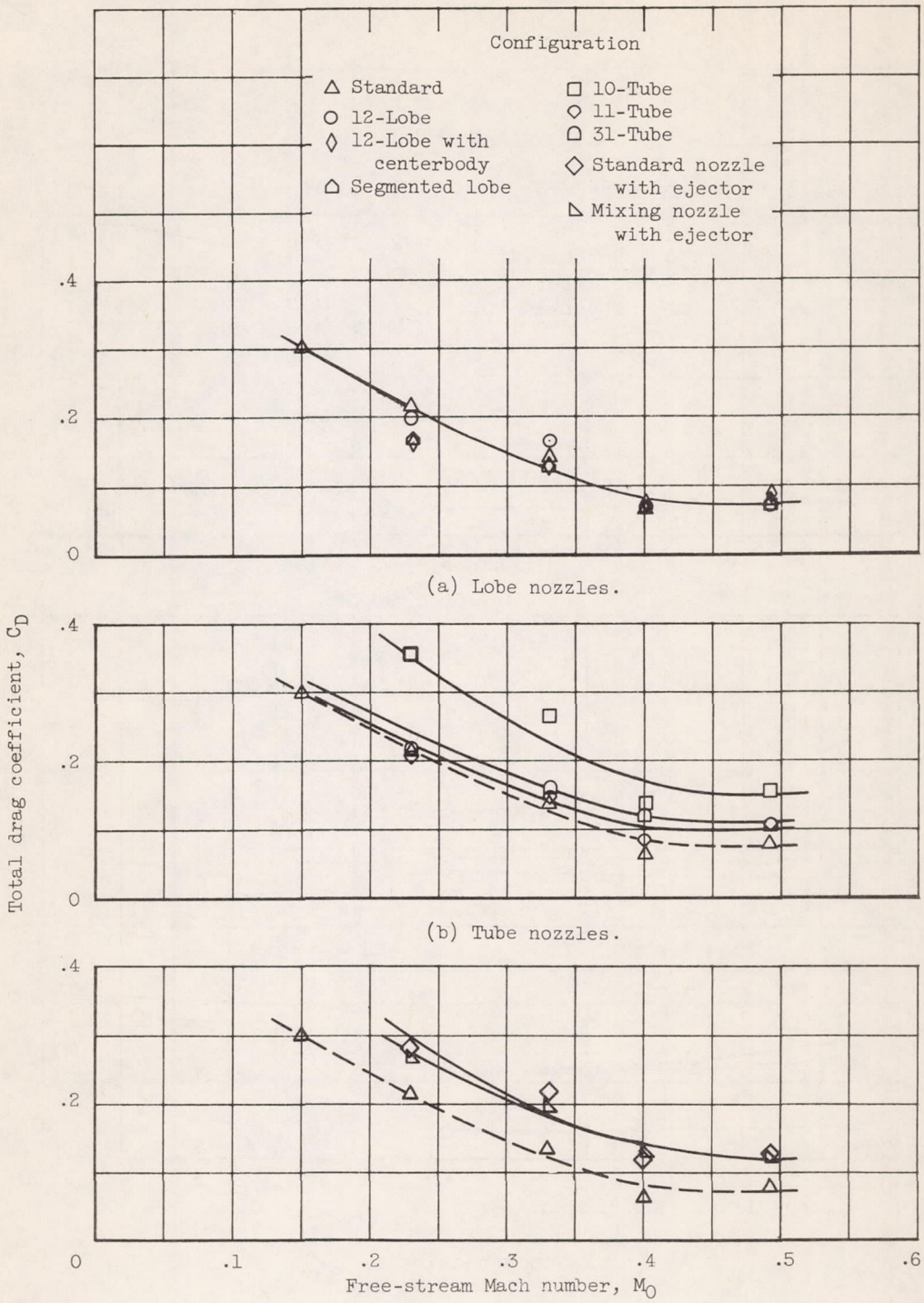

(a) Lobe nozzles.

(b) Tube nozzles.

(c) Ejector nozzles.

Figure 17. - Comparison of total nacelle-drag coefficients of noise-suppressor nozzles and standard nozzle.

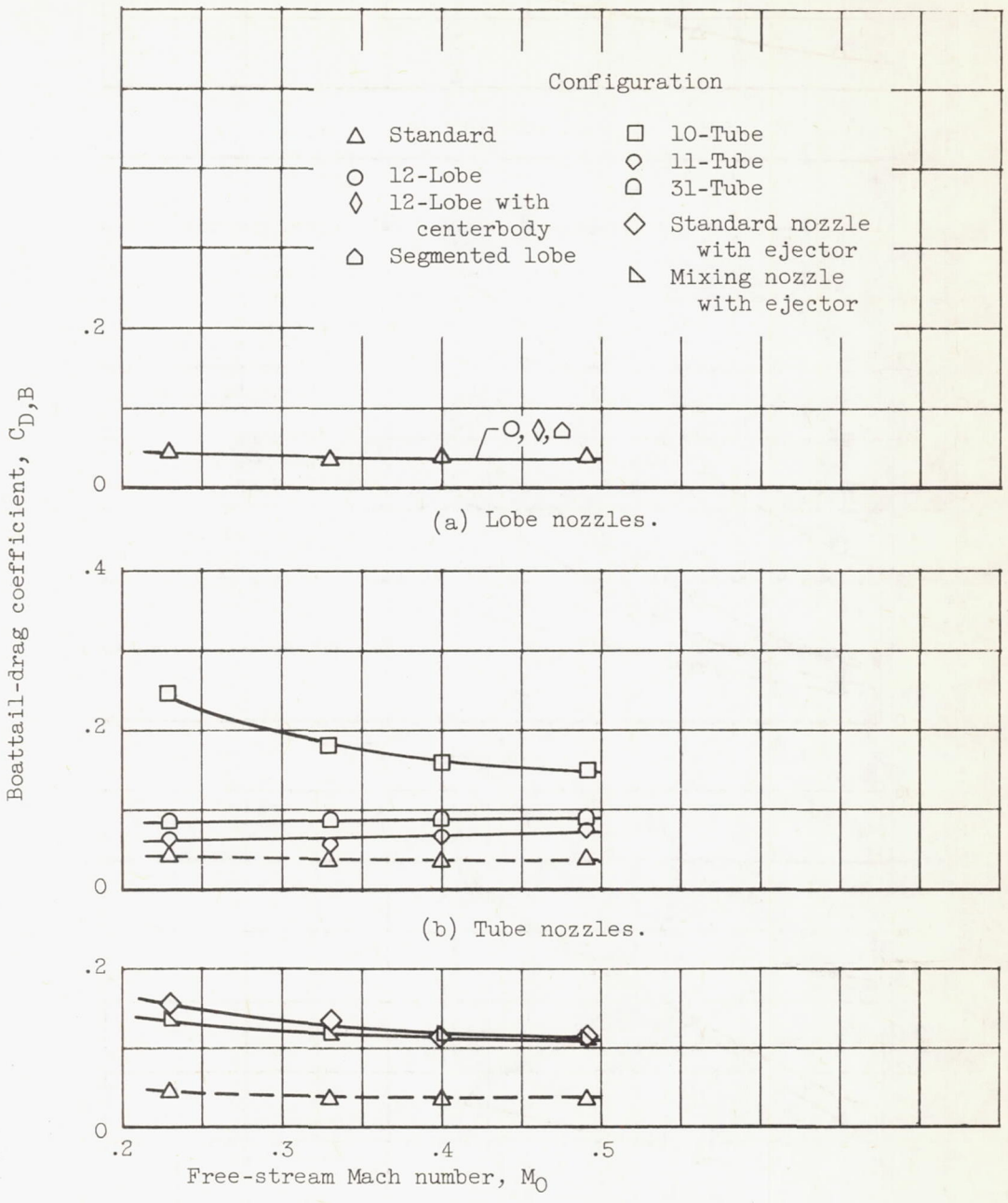

(a) Lobe nozzles.

(b) Tube nozzles.

(c) Ejector nozzles.

Figure 18. - Boattail-drag coefficients of noise-suppressor nozzles and standard nozzle.

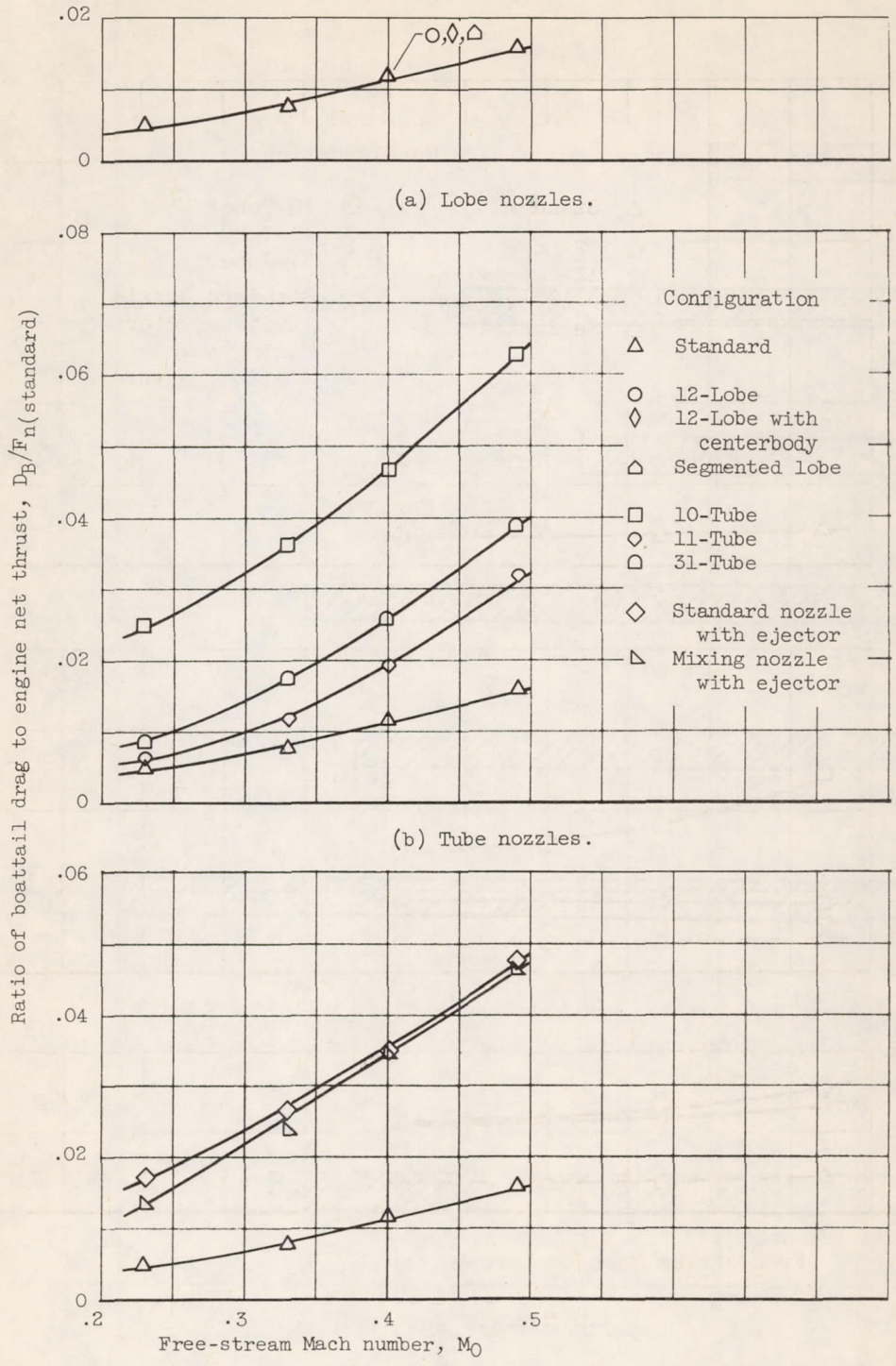

Figure 19. - Ratio of boattail drag to engine net thrust for noise-suppression nozzles and standard nozzle.

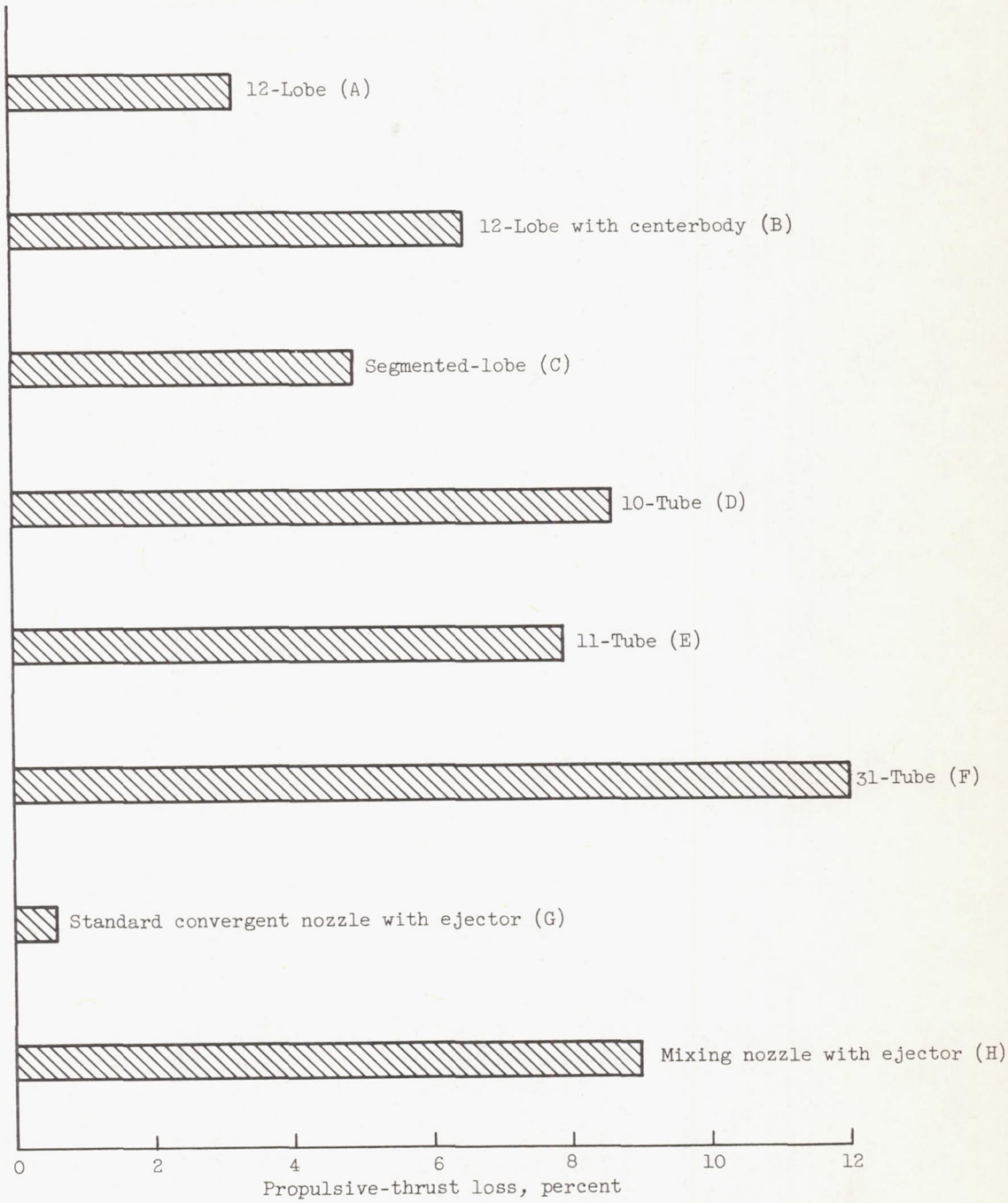

Figure 20. - Comparison of propulsive-thrust losses for noise-suppressor nozzles.